International Journal of Nanomedicine

Dovepress
open access to scientific and medical research

Open Access Full Text Article

ORIGINAL RESEARCH

Curcumin and 5-Fluorouracil-loaded, folate- and transferrin-decorated polymeric magnetic nanoformulation: a synergistic cancer therapeutic approach, accelerated by magnetic hyperthermia

This article was published in the following Dove Press journal:
International Journal of Nanomedicine
9 January 2014
Number of times this article has been viewed

Sivakumar Balasubramanian[1]
Aswathy Ravindran Girija[1]
Yutaka Nagaoka[1]
Seiki Iwai[1]
Masashi Suzuki[1]
Venugopal Kizhikkilot[2]
Yasuhiko Yoshida[1]
Toru Maekawa[1]
Sakthikumar Dasappan Nair[1]

[1]Bio Nano Electronics Research Center, Graduate School of Interdisciplinary New Science, Toyo University, Kawagoe, Japan; [2]Department of Respiratory Medicine, Sooriya Hospital, Chennai, India

Abstract: The efficient targeting and therapeutic efficacy of a combination of drugs (curcumin and 5-Fluorouracil [5FU]) and magnetic nanoparticles encapsulated poly(D,L-lactic-co-glycolic acid) nanoparticles, functionalized with two cancer-specific ligands are discussed in our work. This multifunctional, highly specific nanoconjugate resulted in the superior uptake of nanoparticles by cancer cells. Upon magnetic hyperthermia, we could harness the advantages of incorporating magnetic nanoparticles that synergistically acted with the drugs to destroy cancer cells within a very short period of time. The remarkable multimodal efficacy attained by this therapeutic nanoformulation offers the potential for targeting, imaging, and treatment of cancer within a short period of time (120 minutes) by initiating early and late apoptosis.

Keywords: nanotechnology, curcumin, 5FU, folate, transferrin, PLGA nanoparticle, magnetic hyperthermia

Introduction

Magnetic nanoparticles (MNPs) have arisen as one of the significant innovative nanomaterials that can be used across a range of biomedical applications. Owing to their intrinsic magnetic properties, MNPs have been extensively used for magnetic resonance imaging, magnetic targeting (cell and tissue), magnetic drug delivery, magnetic hyperthermia treatment (MHT), biosensors, magnetofection, and so on.[1–11] Superparamagnetism, a characteristic phenomenon that has been exploited in biomedical research, arises when the size of the MNPs falls lower than 20 nm. Superparamagnetism allows MNPs to gain magnetism in the presence of an applied magnetic field, and they can also lose it when the field is removed.[9,12] The phenomenon of superparamagnetism is extremely beneficial for drug delivery applications. The superparamagnetic iron oxide nanoparticles (SPIONs) can be effectively controlled by external magnets to the targeted tumor area. Upon removal of the external magnetic field, the magnetization of the MNPs disappears; however, MNPs can remain at the target site for a particular period of time. MNPs can be used for diagnostic and therapeutic (theragnostic) purposes in both MHT and chemotherapy, either synergistically or individually.[13,14]

Correspondence: Dasappan Nair Sakthikumar
Toyo University, 2100, Kujirai, Kawagoe, Saitama, 350 – 8585, Japan
Tel +81 492 391 636
Fax +81 492 342 502
Email sakthi@toyo.jp

Compared to the existing anticancer therapies such as chemotherapy and radiotherapy, hyperthermia (specifically MHT) can lower the adverse side effects that this therapy has on normal healthy tissue.[15–19] Generally, hyperthermia can induce whole body or regional heating within the temperature range of 42°C–47°C and the most common means to induce hyperthermia include capacitive or inductive coupling of radiofrequency fields, ultrasound, or microwave.[15–23] Tumor cells are highly heat sensitive compared to normal healthy cells, owing to the fact that the tumor cells are hypoxic while normal cells are euoxic.[17,24] However, unregulated and uncontrolled heating are considered to be the major limitations of hyperthermia, achieved by the methods mentioned previously. With MNPs, much regulated and constant heating can be accomplished by MHT, and the heat can be uniformly affected locally without systemic effects, thus reducing its severe side effects.[25] During MHT with biocompatible magnetic nanoformulation, heat is generated when an alternating current magnetic field is applied. Heat is generated by MNPs depending on the three types of losses, namely hysteresis, Ne'el, and Brownian.[26] SPIONS display Ne'el and Brownian losses, and these losses are responsible for heat generation. The increase in the temperature during MHT chiefly depends on the magnetic properties such as losses and saturation moment, as well as on the frequency and amplitude of the applied field.

Poly(D,L-lactic-co-glycolic acid) (PLGA)-based nanodrug formulations are gaining significant importance in the arena of nanomedicine, owing to its approval by the US Food and Drug Administration.[27–29] Recently, PLGA nanoparticles (NPs) were extensively used for controlled drug release applications under various external stimuli. The present study investigates the concept of a dual targeted PLGA NP system by encapsulating a combination of drugs (curcumin and 5-Fluorouracil [5FU]) and MNPs. Turmeric (*Curcuma longa L.* rhizomes) is an inevitable ingredient in Indian cuisine, and also owing to its immense medicinal potential, it has been used for a long time in Indian medicine for the treatment of several diseases.[30–32] Chemically, curcumin is diferuloylmethane or 1,7-bis(4-hydroxy-3-methoxyphenyl)-1,6-hepadiene-3, 5-dione, and the therapeutic properties of this herb have been accredited to the principal component existing in the rhizome. Curcumin has presented a comprehensive array of pharmacological properties such as anti-inflammatory, antioxidant, anticancer, antimicrobial, antiparasitic, antitumor, anti-angiogenic, and antimutagenic effects.[33,34] Preclinical studies of curcumin have revealed its usage as being the same as excellent therapeutic agents in inhibiting cancer in a variety of cell lines.[32,35–39] Therefore, we chose curcumin as one of the drugs used in our nanoconjugate. 5FU is another highly efficient chemotherapeutic agent that inhibits the methylation reaction of deoxyuridylic acid to thymidylic acid.[40,41] Thus, it interferes with the synthesis of deoxyribonucleic acid and ribonucleic acid. The thymine deficit in the cell intensifies the unbalanced growth and death of the cancer cell.

One of the foremost limitations of prevailing cancer therapies is the lack of specificity of anticancer drug delivery; hence, most anticancer drugs have adverse cytotoxic effects on normal healthy cells. There is an increasing demand for the improvement of the effectual delivery of drugs to the targeted site to achieve the potency of therapeutic agents. There are distinctive features displayed by cancer cells, and researchers are exploiting these exceptional features as preferred targets for a wide variety of biomedical applications.[42,43] Cancer cells often express several normal proteins on the cell surface in greater amounts than the normal cells, and these particular overexpressed proteins on cancer cells are exceptional targets for active targeting. The development of an efficient targeting nanoconstruct can spare the neighboring normal healthy cells to a certain extent. One of the most notable perceptions is the development of multifunctional nanocarriers that comprise a high payload of drugs or imaging moieties, which bind to specific proteins that are overexpressed in cancer cells.[44–46] This can be attained by the formulation of dual-targeting nanoconjugate (folate [F] and transferrin [Tf]). F receptors expressed on the cell membrane are a potential molecular target since they are highly expressed in several carcinomas. Tf, a transmembrane glycoprotein, has been extensively investigated for drug targeting to cancer cells, since most cancer cells overexpress Tf receptors.[47,48] F and Tf receptors are often profusely present on cancer cells with their limited expression on normal healthy cells.[49,50] An additional advantage of the nanosystem was that in addition to the therapeutic efficiency of curcumin, the inherent fluorescence exhibited by curcumin has been used to track the NP inside the cancer cells rather than incorporating a dye. Therefore, the nanoconjugates were used in conjunction with drug load in both diagnostics and therapeutics (theragnostics). We demonstrate that synchronized targeting with these dual targeted particles against cancer cells serve as efficient theragnostic nanotools. Remarkably, we found that these dual targeted/dual drug-loaded and MNP-encapsulated PLGA NPs are extremely specific toward cancer cells, while presenting significant cytotoxicity, thereby showing the prospect for their use in cancer treatment.

The major objectives of the present studies are: 1) to develop dual targeted, dual drug, MNP-encapsulated PLGA nanovectors to examine the antiproliferation of breast cancer cells (MCF7) and glial cells (G1); 2) to study the mechanism of cell death owing to the synergistic effects of the drugs by destabilizing the cytoskeleton and through the loss of mitochondrial membrane potential (MMP); and 3) to investigate the effects of magnetic hyperthermia to exploit the potential of MNPs to destroy cancer cells within a very short period of time.

Materials

Ferrous sulphate hepta-hydrate ($FeSO_4 \cdot 7H_2O$), Ferric chloride hexa-hydrate ($FeCl_3 \cdot 6H_2O$), NaOH, and ethyl acetate were procured from Kanto Chemical (Kanto Chemical Co., Inc., Tokyo, Japan). Folic acid, PLGA, and Tf were purchased from Sigma-Aldrich (St Louis, MO, USA). N-(3-dimethylaminopropyl)-N0-ethylcarbodiimidehydrochloride (EDC) and N-hydroxysuccinimide (NHS) were purchased from Tokyo Chemical Industry Co., Ltd. (Tokyo, Japan) and 5FU was purchased from Nacalai Tesque, Inc. (Kyoto, Japan). Curcumin was gifted from AVT McCormick Ingredients PVT. Ltd. (South Vazhakulam, India). Trypan blue and 0.025% Trypsin were purchased from Sigma-Aldrich. The LIVE/DEAD® Viability/Cytotoxicity Assay Kit, alamarBlue® toxicology kit, 4′,6-diamidino-2-phenylindole (DAPI), and LysoTracker® were purchased from Life Technologies (Carlsbad, CA, USA).

Synthesis of MNPs

SPIONs were synthesized in our laboratory by chemical coprecipitation of iron salts (Fe^{3+} and Fe^{2+}) at a ratio of 2:1 in an ammoniacal medium with magnetic stirring at 80°C in the presence of a nitrogen atmosphere. We have followed previously reported methods for the synthesis of SPIONs.[51,52] Briefly, 0.04 M of $FeCl_3 \cdot 6H_2O$ and 0.02 M of ferrous sulfate ($FeSO_4 \cdot 7H_2O$) were dissolved in a round-bottom flask containing 200 mL of double-distilled water (DDW). The mixture was heated to 80°C with heavy magnetic stirring under the nitrogen atmosphere. To this mixture, 12 mL of a 25% ammonia solution was added. Another 20 minutes of magnetic stirring was continued to stimulate the growth of the NPs, and the mixture was cooled down to normal room temperature. The mixture was further centrifuged and the pellet was washed three times with DDW. By adding dilute HCl, the pH of the suspension was neutralized, and the MNPs were further washed with DDW and dried. The finally obtained dried MNPs were used for further experiments.

Preparation of the dual drug and MNP-encapsulated PLGA NPs

Synthesis of the dual drug and MNP-encapsulated PLGA NPs was carried out by a well-known solvent evaporation technique. The solvent evaporation (single emission) technique is considered to be an effective method for encapsulating hydrophobic drugs.[33] In our study, we have used two drugs: a natural drug (curcumin) and a synthetic drug (5FU). In a typical synthesis, 200 mg of PLGA was dissolved in 2 mL of ethyl acetate solution. In addition, 20 mg of synthesized MNPs, 10 mg of curcumin, and 5 mg of 5FU were added under magnetic stirring, and the stirring was continued for 30 minutes. A total of 5 mL of 5% polyvinyl alcohol was added drop-by-drop, and ultra sonication was given for 2 minutes. The mixture was then added drop-by-drop to 100 mL of a 0.3% polyvinyl alcohol solution, and vigorous magnetic stirring was continued for another 3 hours. The mixture was then centrifuged at 8,000 rpm for 15 minutes and the pellet was washed three times with DDW. The finally obtained dual drug and MNP-encapsulated PLGA NPs (Dd–PLGA–MNPs) were freeze-dried and used for further experiments.

Surface functionalization of Dd–PLGA–MNP

For surface functionalization, 20 mg of Dd–PLGA–MNPs were dissolved in 10 mL of 0.02 M pH 7.4 phosphate buffered saline (PBS) buffer. The NP was activated by adding a 1 mg/mL concentration of 250 µL of EDC and a 1 mg/mL concentration of 250 µL of NHS under magnetic stirring for 3 hours.[53] After stirring, the sample was centrifuged and the pellet was washed with PBS buffer to eliminate the unreacted EDC and NHS. The pellet was resuspended in 3 mL of pH 7.4 PBS buffer. Tf and F (200 µL of 1 mg/mL) was added under magnetic stirring for 2 hours, followed by overnight incubation at 4°C in a refrigerator. After the incubation period, the mixture was centrifuged and the pellet was washed three times with pH 7.4 PBS buffer. Finally, double-targeted Dd–PLGA–MNPs (Dt–Dd–PLGA–MNPs) were obtained and used for further experiments.

Physicochemical characterization of NPs

The internal structures of MNPs and Dt–Dd–PLGA–MNPs were characterized by JEM-220-FS field-emission transmission electron microscope (TEM) (JEOL, Tokyo, Japan). Preparation of the TEM samples was carried out by adding the diluted samples into hydrophilic carbon-coated copper grids. Prior to the addition of the samples, the grids were given hydrophilic treatment using a JEOL Datum HDT-400

device. The elemental analysis of the samples was determined by TEM–energy-dispersive X-ray spectroscopy (JEOL JED-2300T; JEOL). Surface morphology of the NPs was carried out by scanning electron microscope (SEM) (JEOL JSPM-6490; JEOL). The sample used for the SEM was diluted by DDW, dropped into silica substrate, dried under vacuum, and used for SEM analysis. Dt–Dd–PLGA–MNPs were further characterized using atomic force microscopy (AFM). The tapping mode of the cantilever was used in the AFM analysis of NPs (MFP-3D-CF™ AFM, Asylum Research, Santa Barbara, CA, USA). A sample solution (200 µL) was deposited on a glass surface, vacuum-dried, and was used for AFM analysis. The surface elemental analysis of the samples for the confirmation of the targeting agents was performed by an X-ray photoelectron spectrometer (XPS) system (Kratos Axis, Shimadzu Corp, Tokyo, Japan). The diluted samples were placed in a silicon substrate and dried, and the samples were characterized. Vibrating sample magnetometer (VSM) measurement of the MNPs and of the Dt–Dd–PLGA–MNPs was performed using VSM model 7407 (Lakeshore Cryotronics, Inc., Westerville, OH, USA).

The encapsulation efficiency of curcumin and 5FU

Encapsulation efficiencies of the Dt–Dd–PLGA–MNPs were carried out by an indirect technique. Briefly, 1 mg of Dt–Dd–PLGA–MNPs was centrifuged at 10,000 rpm for 30 minutes. The supernatant was collected and the obtained pellet was further washed with DDW. Absorbance of the collected supernatant was checked and recorded at 430 nm for curcumin and at 265 nm for 5FU. Based on the standard curve of curcumin and 5FU, the absorbance value of the free drug concentration was calculated. Drug encapsulation efficiency percentage was estimated by a formula that is given below:

$$\text{Encapsulation efficiency}\,(\%) = \frac{D_T - D_F}{D_T} \times 100 \quad (1)$$

where D_T is the total drug and D_F is the free drug present in the supernatant.

Drug release profile of curcumin and 5FU

The drug release profile of curcumin and 5FU from Dt–Dd–PLGA–MNPs in PBS at different pH levels (pH 7.4 and pH 4.5) was studied. A total of 10 µg of the samples was dispersed into 50 mL of PBS buffer at pH 7.4 and pH 4.5. The sample was kept in a water bath shaker with 120 rpm of shaking speed at 37°C. At specific time intervals, 3 mL of supernatant from the sample was collected, and in combination with 3 mL of fresh PBS buffer, was added to compensate for the loss. The absorbance of the collected sample was recorded at 265 nm for 5FU and 430 nm for curcumin. The in vitro drug release profile was calculated by the following formula:

$$\text{Drug release}\,(\%) = \frac{D_R}{D_T} \times 100, \quad (2)$$

where D_R is the concentration of the drug released at collected time (t) and (D_T) is the total amount of the drug that was encapsulated in the NPs.

Cell studies

Cell culture maintenance

A human breast cancer cell line (MCF7 cells), a human glial cell line (G1 cells), and a mouse fibroblast cell line (L929 cells) were cultured for in vitro experimental studies. The cell lines were procured from the Riken Culture Collection Center (RIKEN BioResource Center, Ibaraki, Japan). All of the cell lines were grown in Dulbecco's Modified Eagle's Medium (DMEM) with 10% heat-inactivated fetal bovine serum and penicillin/streptomycin (100 units/mL) in T25 flasks and maintained at 37°C in a humidified 5% CO_2 atmosphere. The cells were subcultured every 2 days. The cells were maintained in glass-base dish for confocal studies, six-well plates for flow cytometry studies, 96-well plates for cytotoxicity studies, and in 35 mm plates for MHT studies.

Biocompatibility studies

NP samples (bare MNPs and PLGA–MNPs) were prepared and diluted to different concentrations (0.1 mg/mL, 0.5 mg/mL, and 1 mg/mL) with PBS (pH 7.4) for treatment in 96-well tissue culture plates for studying the biocompatibility of the NPs in the three different cell lines. An alamarBlue assay was performed to investigate the cell viability. The alamarBlue assay is based on the natural reducing ability of the healthy cells to convert resazurin to a fluorescent molecule, resorufin. The assay indicates the active metabolism that is happening inside of the cell, and the active metabolism diminishes when the NP sample triggers toxicity, which leads to decreased reduction capability. The fluorescence intensity based on the alamarBlue assay was quantified at 580–610 nm in a multidetection microplate reader (Power Scan HT, Dainippon Sumitomo Pharma Co., Ltd., Osaka, Japan).

Internalization studies of NPs

The internalization of NPs by MCF7, G1, and L929 was studied using cellular imaging by confocal microscopy and flow cytometry. The intrinsic fluorescence of curcumin was exploited for labeling the cells and, hence, for monitoring the uptake of NPs by confocal microscopy. A human breast cancer cell line (MCF7 cells), a human glial cell line (G1 cells), and a mouse fibroblast cell line (L929) were routinely grown in DMEM, as mentioned, on a glass-base dish for 24 hours for the imaging studies. We examined the uptake of single targeted NPs (F and Tf, separately) and Dt–Dd–PLGA–MNPs. After incubation, the cells were washed with PBS, and 20 µL of the NP samples, F–Dd–PLGA–MNPs, Tf–Dd–PLGA–MNPs, and Dt–Dd–PLGA–MNPs suspended in culture medium, were added. The cells were incubated with NPs for 4 hours to analyze their cellular uptake. After incubation, the culture medium with the NPs was removed and the cells were washed twice with PBS buffer, and the nucleus was stained with DAPI. Also, to confirm the endosomal-mediated uptake of the NPs, we performed LysoTracker staining to map the lysosomes of the cells that were viewed under confocal microscopy (Olympus IX81 in DU897 mode; Olympus Corporation, Tokyo, Japan).

The cellular uptake of the NPs (F–Dd–PLGA–MNPs, Tf–Dd–PLGA–MNPs, and Dt–Dd–PLGA–MNPs) was further confirmed using flow cytometry (JSAN™ cell sorter; Bay bioscience Co., Ltd., Kobe, Japan). MCF7, G1, and L929 were plated at a density of 2.5×10^6 cells per well. After attaining 80% confluency, 200 µg/mL of the NPs was added and incubated for 4 hours. After the specified incubation period, the cells were washed three times with PBS to remove any unbound NPs. The cells were trypsinized and resuspended in 500 µL of cold PBS. A total of 500 µL of 3% paraformaldehyde was used to fix the cells, and the cells were incubated for 20 minutes. After fixation, the cells were again washed with cold PBS and permeabilized with 500 µL of ice-cold methanol, and incubated for another 10 minutes. Cold PBS (500 µL) was added to the cells after incubation, and the cells were again washed with PBS and finally resuspended in 500 µL of PBS. Flow cytometry of the cells was performed in a fluorescein isothiocyanate (FITC) channel, and data were analyzed using JSAN™ App San software (Bay bioscience, Co., Ltd.) to study the uptake of the NPs by the cell lines.

Therapeutic efficiency against cancer cells by nanoformulation

The therapeutic effect of targeted drug-loaded nanoformulations on cell proliferation was determined by alamarBlue colorimetric assay. Briefly, cancer cells (MCF7 and G1) and control cells (L929) were seeded in 96-well plates at a density of 5,000 cells per well. After the overnight incubation at 37°C, cells were treated with varying concentrations of NPs. For the antiproliferative effect of NPs, we studied the cytotoxic effects of dual-targeted, single-drug-loaded NPs (Dt-Cur-PLGA-MNPs and Dt–5FU–PLGA–MNPs) and nontargeted NPs with a combination of the drug (Dd–PLGA–MNP) and Dt–Dd–PLGA–MNPs. Cell viability was determined up to 96 hours following NP treatment using alamarBlue assay. Determination of the cell viability in the presence of drug-loaded NPs indirectly quantifies the cytotoxicity caused by these NPs. All the experiments were performed in triplicate. The cells were also plated on six-well plates to examine the therapeutic efficacy of Dt–Dd–PLGA–MNPs by phase contrast microscopy.

Mode of cellular death induced by Dt–Dd–PLGA–MNPs

Mitochondrial depolarization studies

The effect of Dt–Dd–PLGA–MNP nanoformulation on membrane potential was studied by mitochondrial membrane depolarization on MCF7 and G1 cells. Briefly, the cells were grown in a glass-based dish and an appropriate amount of Dt–Dd–PLGA–MNPs was treated and incubated at 37°C for 24 hours. The cells were washed with cold PBS three times to remove unbound NPs, and they were then stained with cationic dye JC-1. The cells stained with the dye were incubated for 15 minutes at 37°C to permit a potential-dependent accumulation of the dye in the mitochondria of the cells. In normal healthy cells, owing to the electrochemical potential gradient, JC dye accumulates in the mitochondrial matrix, where it forms red fluorescent aggregates and provides bright red fluorescence. Curcumin in the nanoformulation degenerates the MMP and prevents the accumulation of the JC-1 dye in the mitochondria. Thus, the dye is distributed throughout the entire cell resulting in a shift from red to green fluorescence of the JC-1 monomers. After 15 minutes, the cells were washed with PBS twice and viewed under confocal microscopy (Olympus IX81 under DU897 mode).

Cytoskeletal destabilization by Dt–Dd–PLGA–MNPs

To study the effect of Dt–Dd–PLGA–MNPs on the cytoskeletal organization of cells, confocal microscopy analysis of the cancer cells was performed in MCF7 and G1 cells. MCF7 and G1 cells were cultured on glass-base dishes for 24 hours prior to NP treatment and the cells were incubated for 48 hours. After incubation, the cells were washed three times with PBS

to remove unbound NPs. The cells were stained with tubulin and actin markers and viewed under a confocal microscope (Olympus IX81 in DU897 mode) using a 100 × oil objective and 488/561 nm excitation.

Determination of apoptosis induced by nanoformulation

Apoptosis includes a series of highly orderly events associated with programmed cell death that is depicted by definite features such as shrunken cell morphology, membrane blebbings, nuclear condensation, appearance of blisters, and so on. On the other hand, necrosis is cell death stimulated by external damage, and the necrotic cells are characterized by the distorted cell structure and lysis of the plasma membrane, and by the incidence of swollen nuclei without condensed chromatin, thus leading to cell death. The apoptotic population of cells when treated with Dt–Dd–PLGA–MNPs was determined by flow cytometry and confocal microscopy with the Annexin V-FITC and propidium iodide apoptosis kit (Sigma-Aldrich). For flow cytometry, cells were grown in six-well plates at a density of 2.5×10^6 cells, treated with an appropriate concentration of Dt–Dd–PLGA–MNPs. After incubation, the cells were washed with PBS and resuspended in 1X binding buffer. A total of 5 µL of Annexin V-FITC conjugate and 10 µL of propidium iodide solution were added to each cell suspension. The cells were incubated at room temperature for 10 minutes and protected from light. Fluorescence of the cells was determined by flow cytometry. For qualitative determination, cells were grown in a glass-base dish and incubated overnight at 37°C. The next day, the medium was removed, and fresh medium containing Dt–Dd–PLGA–MNPs was added. After the incubation, the cells were washed thrice with PBS. Subsequently, the cells were stained with Annexin V conjugate and PI, based on the manufacturer's protocol. The images were viewed under confocal microscopy (Olympus IX 81 under DU897 mode).

MHT-based cytotoxicity studies

In order to study the synergistic effect of the encapsulated drug in our nanoformulation, we performed a drug release study under a magnetic field. Dt–Dd–PLGA–MNPs of different pH levels (7.4 and 4.5) were subjected to an alternating current (AC) magnetic field (H=18.03 kA/m; B=166.25 A; frequency =305 KHz) for 60 minutes and 120 minutes, and the percentage of drug release was quantified. We have exploited the magnetic potential of the nanoformulation by performing MHT on control (L929) and cancer cells (MCF7 and G1). The cells for the MHT studies were seeded at a density of 1.6×10^5 cell/mL in 35 mm tissue culture dishes. After attaining 80% confluency, the culture was replenished with a fresh medium containing 1 mg/mL of Dt–Dd–PLGA–MNPs. The cells were incubated for 4 hours and after incubation, the cells were washed three times with PBS to remove unbound NPs. The NP-internalized cells were exposed to the AC magnetic field (H =18.03 kA/m; B =166.25 A; frequency =305 KHz) for 60 minutes and 120 minutes. After treatment, the cells were harvested by trypsinization (0.025% trypsin for 5 minutes), and counted in the presence of Trypan blue to determine cell viability. The viability of the cells that were exposed to the magnetic field was compared with that of the control cells at 37°C, which were not treated with the NP suspension or exposed to the magnetic field. The experiments were done in triplicate.

The effect of incubation time on the viability of the cancer cells after MHT was studied by incubating the cells in a CO_2 incubator at 37°C for varying periods of time (12 hours and 24 hours). The number of cells was counted to determine the change in the viability of cells with different incubation periods. The viability of the MHT-treated cells was compared to that of the control cells at 37°C; the control cells were not treated with a NP suspension or exposed to a magnetic field. The experiments were done in triplicate.

Cytoskeletal destabilization by Dt–Dd–PLGA–MNPs induced by MHT

To study the effect of MHT on the cytoskeletal organization of cells and to study the mechanisms of cell death induced by nanoformulation, confocal microscopy analysis of the cancer cells treated with targeted NPs was performed. MCF7 and G1 cells were cultured on glass-base dishes for 24 hours prior to NP treatment. The cells with the nanoformulation were exposed to the AC magnetic field (H =18.03 kA/m; B =166.25 A; frequency =305 KHz) for 120 minutes. After treatment, the cells were washed three times with PBS to remove unbound NPs. The cells were stained with tubulin and actin markers, and were viewed under a confocal microscope (Olympus IX81 in DU897 mode) using a 100 × oil objective and 488/561 nm excitation.

Qualitative determination of LIVE/DEAD cells after MHT

The LIVE/DEAD Viability/Cytotoxicity Assay Kit was used for the simultaneous determination of live and dead cells after MHT on the cancer cells. Briefly, MCF7 and G1 cells were grown in a glass-base dish for 24 hours with standard medium and the cells were then replenished with fresh medium containing Dt–Dd–PLGA–MNPs. The cells were exposed to the AC magnetic field (H =18.03 kA/m; B

=166.25 A; frequency =305 KHz) for 120 minutes. Following hyperthermia, the cells were washed in cold PBS to remove unbound NPs, and they were then stained with the reagents in the LIVE/DEAD viability kit. The images were viewed under confocal microscopy (Olympus IX81 under DU897 mode).

Results and discussion

We have successfully encapsulated MNPs and two potential drugs, curcumin and 5FU, into a biodegradable PLGA polymer by the solvent evaporation technique, as depicted in Figure 1A. The specificity for the nanoconjugate was imparted by two targeting moieties, F and Tf via an EDC/NHS coupling reaction as represented in Figure 1B. Thus, the targeted nanoconjugate (Dt–Dd–PLGA–MNPs) could deliver the therapeutic agents to the cancer cells, and these agents could be proficiently internalized into the cancer cells through receptor-mediated endocytosis.

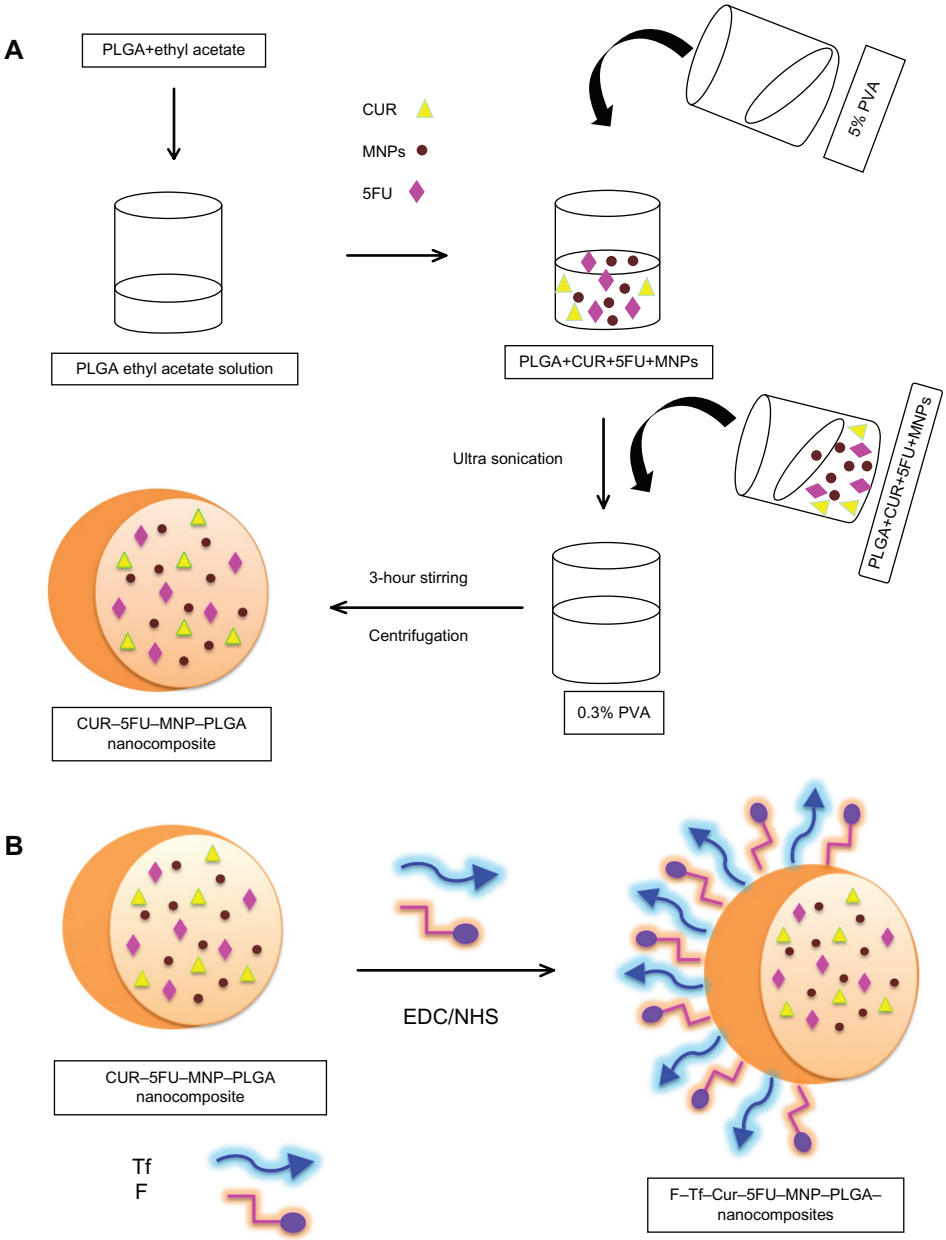

Figure 1 Schematic of the synthesis of Dd–PLGA–MNPs and biofunctionalization of NPs with F and Tf to form Dt–Dd–PLGA–MNPs.
Notes: (**A**) Schematic of synthesis of Dd–PLGA–MNPs; (**B**) biofunctionalization of NPs with F and Tf to form Dt–Dd–PLGA–MNPs.
Abbreviations: PLGA, poly(D,L-lactic-co-glycolic acid); CUR, curcumin; MNP, magnetic nanoparticle; 5FU, 5-Fluorouracil; PVA, polyvinyl alcohol; EDC, N-(3-dimethylaminopropyl)-N0-ethylcarbodiimidehydro-chloride; NHS, N-hydroxysuccinimide; F, folate; Tf, transferrin; NPs, nanoparticles; Dd–PLGA–MNPs, double drug loaded magnetic nanoparticle-encapsulated poly(D, L-lactic-co-glycolic acid) nanoparticles; Dt–Dd–PLGA–MNPs, double targeted double drug loaded magnetic nanoparticle-encapsulated poly(D, L-lactic-co-glycolic acid) nanoparticles.

The TEM observations of the plain MNPs and PLGA–MNPs are shown in Figure 2A and B. We have observed smooth and spherical MNPs with an average size in the range of 10±3 nm. By TEM analysis, PLGA–MNPs exhibited multiple MNPs encapsulated into a single PLGA NP and revealed high monodispersity, devoid of any aggregation with an average size of 150 nm. The presence of multiple MNPs in single PLGA NP could augment the magnetization responsiveness of nanoconjugate for magnetism-related studies. Energy-dispersive X-ray spectroscopy analysis was performed to check for the presence of Fe, C, and O in the MNPs and PLGA–MNPs (Figure 2C and D). SEM analysis of the PLGA–MNPs also supported the TEM observations, as the PLGA–MNPs were monodisperse, uniform, spherical, and smooth surfaced, with an average size of 150 nm (Figure 2E). The AFM image of the NPs that was taken under high resolution also displayed a smooth surface and had a uniform size distribution of 150 nm (Figure 2F).

To confirm the attachment of targeting ligands (F and Tf) onto Dd–PLGA–MNPs, XPS was carried out. For the XPS studies, we analyzed Dd–PLGA–MNPs and Dt–Dd–PLGA–MNPs, and the result is provided in Figure 3. In the case of Dt–Dd–PLGA–MNPs, C and N peaks along with Si and O (arising from substrate) were seen. The N peak is from the conjugated biomoieties (F and Tf) on Dt–Dd–PLGA–MNPs, thus providing evidence for the appropriate functionalization and conjugation of the targeting moieties on the NPs. In the case of Dd–PLGA–MNPs, the N peak was absent, signifying

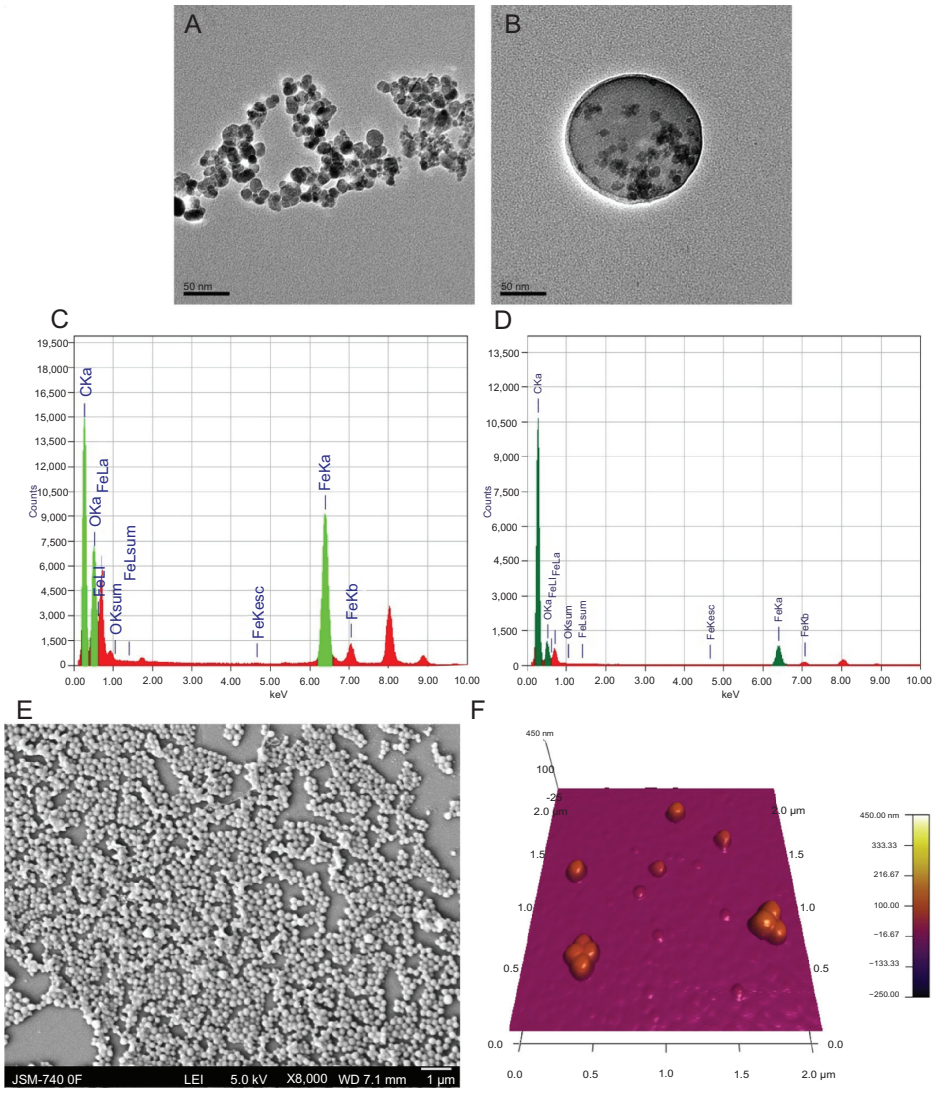

Figure 2 TEM, TEM–EDS, SEM, and AFM images of MNPs and PLGA–MNPs.
Notes: (**A** and **B**) TEM image of MNPs and PLGA–MNPs; (**C** and **D**) TEM–EDS of MNPs and PLGA–MNPs; (**E**) SEM of PLGA–MNP; (**F**) AFM of PLGA–MNP.
Abbreviations: TEM, transmission electron microscopy; EDS, energy-dispersive X-ray spectroscopy; SEM, scanning electron microscopy; AFM, atomic force microscopy; MNP, magnetic nanoparticle; PLGA, poly(D,L-lactic-co-glycolic acid).

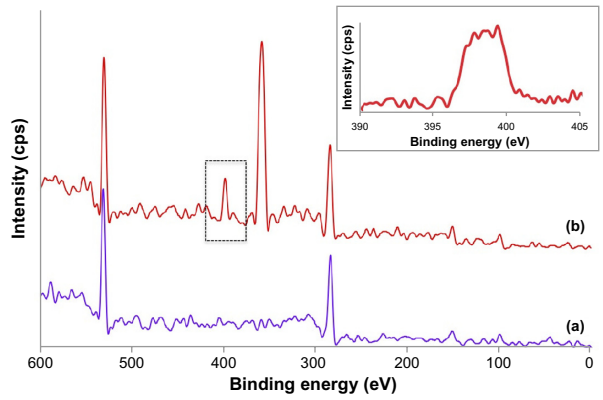

Figure 3 XPS elemental analysis spectra for Dd–PLGA–MNPs and Dt–Dd–PLGA–MNPs. Inset corresponds to N 1 s peak, which indicates bioconjugation.
Notes: (a) represents Dd–PLGA–MNPs and (b) represents Dt–Dd–PLGA–MNPs.
Abbreviations: XPS, X-ray photoelectron spectrometer; Dd–PLGA–MNPs, double drug loaded magnetic nanoparticle-encapsulated poly(D, L-lactic-co-glycolic acid) nanoparticles; Dt–Dd–PLGA–MNPs, double targeted double drug loaded magnetic nanoparticle-encapsulated poly(D, L-lactic-co-glycolic acid) nanoparticles.

the absence of biofunctionalization. Also, the absence of the Fe peak clearly indicated that MNPs and the drug were entrapped inside the PLGA NPs.

The magnetic property of bare MNPs and Dt–Dd–PLGA–MNPs was investigated in VSM at 300 K, and the acquired results are shown in Figure 4. From the results, it was observed that the remanent magnetization and coercivity were close to zero, which clearly signified the characteristic of superparamagnetism. The slight decrease in magnetization for Dt–Dd–PLGA–MNPs can be attributed to the PLGA coating. We could also observe that an external magnet could easily affect the magnetic behavior of the Fe_3O_4 core, and these conjugates can be efficiently manipulated by an external magnetic field, for example, in MHT.[54]

A key prerequisite for any nanocarrier is its high drug-loading capacity, which could reduce the quantity of carriers that are necessary for its drug delivery application. In our study, we could attain an efficient loading of drugs (curcumin and 5FU) into PLGA NPs. The percentage of the drug loaded into the PLGA NPs was quantified spectrophotometrically with ultraviolet–visible spectroscopy absorption by attaining the absorption values of the standard drug concentrations. The encapsulation efficiency of curcumin and 5FU within the PLGA NPs was 71% and 63%, respectively. The steady and sustained release of the entrapped drug from the NPs is a vital consideration for the efficacious development of nanoformulations for biomedical applications. The sensitivity of polymeric NPs to physiological changes (such as pH, temperature, and external stimuli that stimulate a sustained release of the therapeutic agent) is gaining greater significance.[55] We studied the release of a combination drug

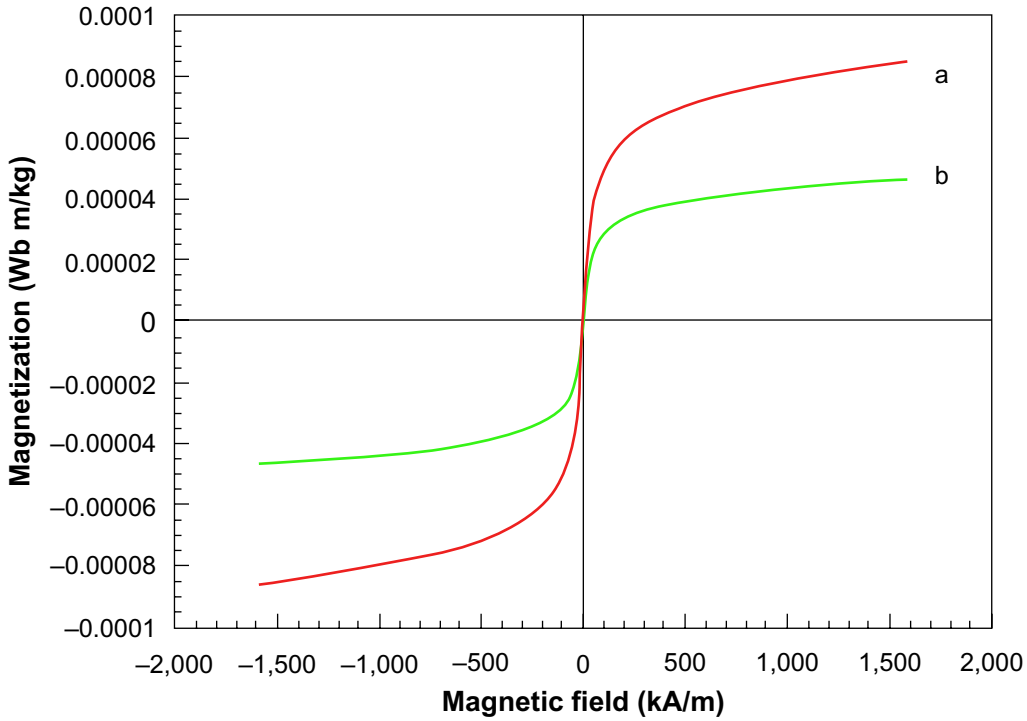

Figure 4 Magnetization versus magnetic field for the samples.
Notes: (a) represents MNPs and (b) represents Dt–Dd–PLGA–MNPs.
Abbreviations: MNPs, magnetic nanoparticles; Dt-Dd-PLGA-MNPs Double targeted double drug loaded magnetic nanoparticle-encapsulated poly(D, L-lactic-co-glycolic acid) nanoparticles.

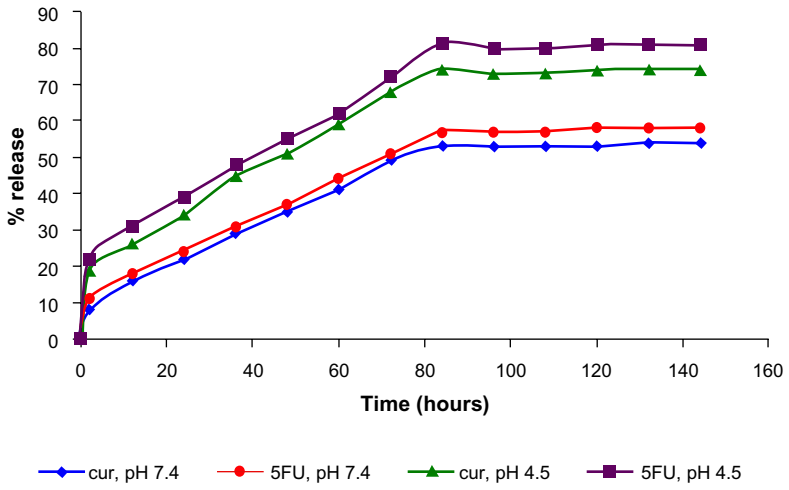

Figure 5 In vitro release of Cur and 5FU from Dt–Dd–PLGA–MNPs in phosphate buffered saline at different pH levels (4.5 and 7.4).
Abbreviations: Cur, curcumin; 5FU, 5-Fluorouracil; Dt–Dd–PLGA–MNPs, double targeted double drug loaded magnetic nanoparticle-encapsulated poly (D, L-lactic-co-glycolic acid) nanoparticles.

encapsulated in PLGA NPs in two different pH levels (4.5 and 7.4), corresponding to the acidic condition in endosomes and the physiological pH, respectively. At different time intervals, the released drug at pH levels of 7.4 and 4.5 was collected and the supernatant was analyzed. We observed a pH responsive difference in the release of drugs from NPs. As displayed in Figure 5, the release profile of the drugs (curcumin and 5FU) in combination with the nanoformulation exhibited a sustained release pattern, which was illustrated by a slower and sustained release over 144 hours. The release kinetics at pH 4.5 and 7.4 within 144 hours indicated that pH strongly influenced the release of both drugs from the PLGA NPs. We have observed a release of more than 70% of curcumin and more than 80% of 5FU in a period of 144 hours in a pH level of 4.5. Among the two different pH conditions studied, the drug release during the acidic conditions showed a greater percentage of release of the encapsulated drugs, which supports the drug's efficiency as an anticancer therapy.

The biocompatibility of MNP–PLGA was studied in normal mouse fibroblast cells (L929), a human breast adenocarcinoma cell line (MCF7), and a human glial cell line (G1) for 24 hours; an alamarBlue assay was performed and the results are shown in Figure 6. When the cells were treated with bare MNPs at the highest concentration of 1 mg/mL, the viability was found to be 51%, 57%, and 53% for L929, G1 and MCF7 respectively. The cellular viability was significantly augmented to 90%, 89%, and 86% in L929, MCF7, and G1, respectively, when treated with the highest concentration (1 mg/mL) of PLGA–MNPs; this indicated the biocompatibility of the MNPs within PLGA NPs. The observed results confirmed the application of PLGA-coated MNPs for the safe delivery of encapsulated therapeutic agents, as well as for their use in MHT studies.

Internalization studies of nanoparticles

The internalization of single- or dual-targeted dual drug-loaded PLGA–MNPs in cancer cells (MCF7 and G1) and in control cells (L929) was examined by confocal laser scanning

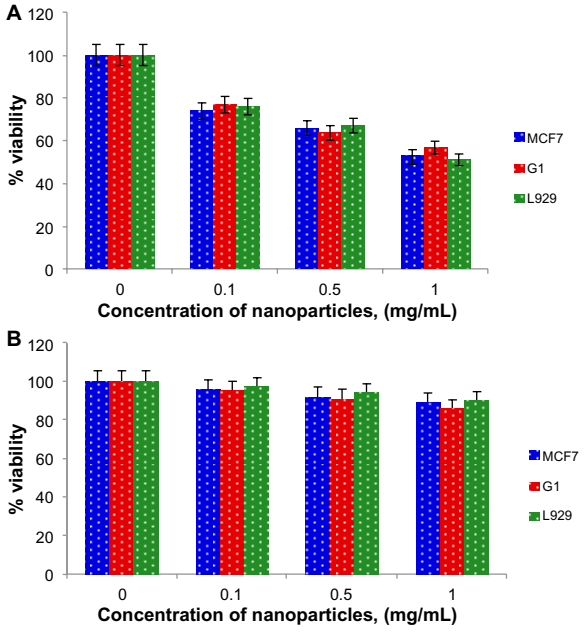

Figure 6 The alamarBlue assay results for the cytotoxicity of bare MNPs and biocompatibility of PLGA–MNPs on the MCF7, G1, and L929 cell lines.
Notes: (**A**) Cytotoxicity of bare MNPs and (**B**) Biocompatibility of PLGA–MNPs on the MCF7, G1, and L929 cells at various concentrations.
Abbreviations: MNPs, magnetic nanoparticles; PLGA, poly(D,L-lactic-co-glycolic acid).

microscopy (CLSM). The fluorescence signal from curcumin was used to study the uptake of the NPs. In the case of single-targeted NPs (either F or Tf) in MCF7 and G1 cells, the intake of the NPs was evident, and this is largely due to the existence of targeting ligands, F or Tf, both being highly expressed abundantly in cancer cell lines. However, individual single-targeted NPs exhibited comparably equal internalization by cancer cells, and the fluorescence signal was not very strong. However, the cells treated with dual-targeted NPs exhibited the highest level of NP accumulation in the cell cytoplasm, and this was observed in MCF7 and G1 cells, emphasizing the enhanced uptake by dual-targeted NPs (Figure 7A). The uptake of NPs can be attributed to F and Tf receptor-mediated endocytosis by the cancer cell lines. Thus, our confocal observation demonstrates that dual-targeted NPs were highly specific for cancer cells that were internalized more than single-targeted NPs (either F or Tf). The results clearly described that targeted NPs were efficient in cancer cell targeting and internalization, with the dual-targeted NPs exhibiting enhanced and efficient uptake by the cancer cells.

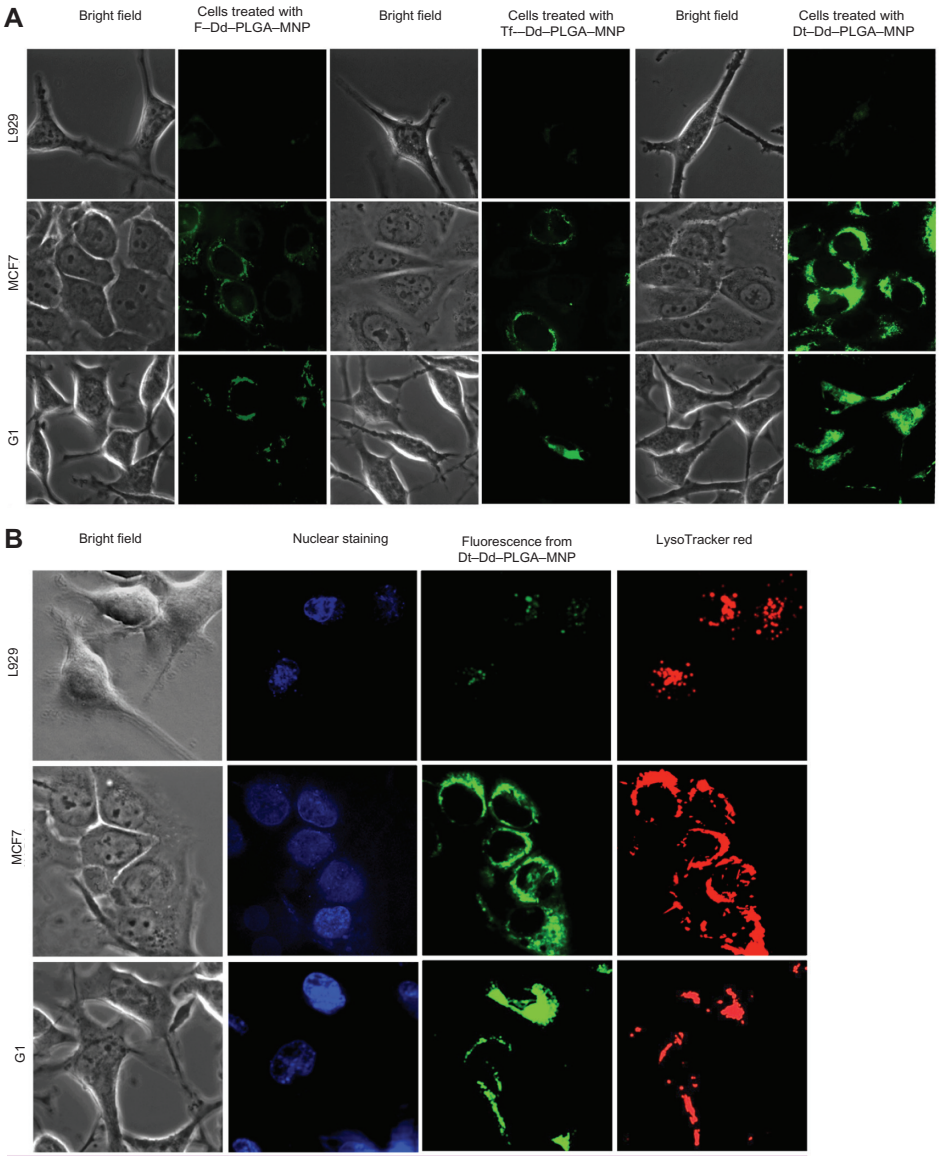

Figure 7 Internalization of NPs by L929, MCF7, and G1 cells, as well as uptake of Dt–Dd–PLGA–MNPs and co-localization studies.
Notes: (**A**) Internalization of NPs (F–Dd–PLGA–MNPs, Tf–Dd–PLGA–MNPs, and Dt–Dd–PLGA–MNPs) by L929, MCF7 and G1 cells. The fluorescent intensity of Dt–Dd–PLGA–MNPs in cancer cells was stronger than the other nanoformulations studied signifying the efficacy of dual-targeted NPs. (**B**) Uptake of Dt–Dd–PLGA–MNPs and co-localization studies with LysoTracker red indicating presence of NPs in the lysosome.
Abbreviations: F–Dd–PLGA–MNPs, folate targeted double drug loaded magnetic nanoparticle-encapsulated poly(D, L-lactic-co-glycolic acid) nanoparticles; Tf–Dd–PLGA–MNPs, transferrin targeted double drug loaded magnetic nanoparticle-encapsulated poly(D, L-lactic-co-glycolic acid) nanoparticles; Dt–Dd–PLGA–MNPs, double targeted double drug loaded magnetic nanoparticle-encapsulated poly(D, L-lactic-co-glycolic acid) nanoparticles.

When the single- and dual-targeted NPs were treated with control (mouse fibroblast) L929 cells, none of the targeted NPs was efficiently internalized, and hence the fluorescence signal was not observed (Figure 7A). Although L929 cells also expresses F and Tf receptors, the expression of the receptors are under the threshold level for normal functioning of the cell. These results clearly indicated the attainment of the highly specific targeting directed towards the cancer cells. To confirm the endosome-mediated entry of NPs, lysosomal staining was performed with LysoTracker red. The overlapping signal of the green fluorescent signal from curcumin and the red signal from lysosomes confirmed the presence of NPs in the lysosome (Figure 7B).

To validate the enhanced uptake of Dt–Dd–PLGA–MNPs by the cancer cells, we have compared the cellular uptake of single-targeted NPs (F–Dd–PLGA–MNPs and Tf–Dd–PLGA–MNPs) by flow cytometry. Cancer cells (MCF7 and G1) and the control cell line (L929) cells were incubated with NPs for 4 hours. In the case of cancer cells, the fluorescent intensity profile of Dt–Dd–PLGA–MNPs increased by ten times that of the single-targeted NPs, signifying the enhanced receptor-mediated uptake of NPs; this resulted in the increased internalization of the NPs into the cells (Figure 8). Furthermore, we incubated the normal cells (L929) with single-targeted and double-targeted NPs, and flow cytometry was carried out. The results, as represented in Figure 8, denote that the fluorescence intensity of L929 cells incubated

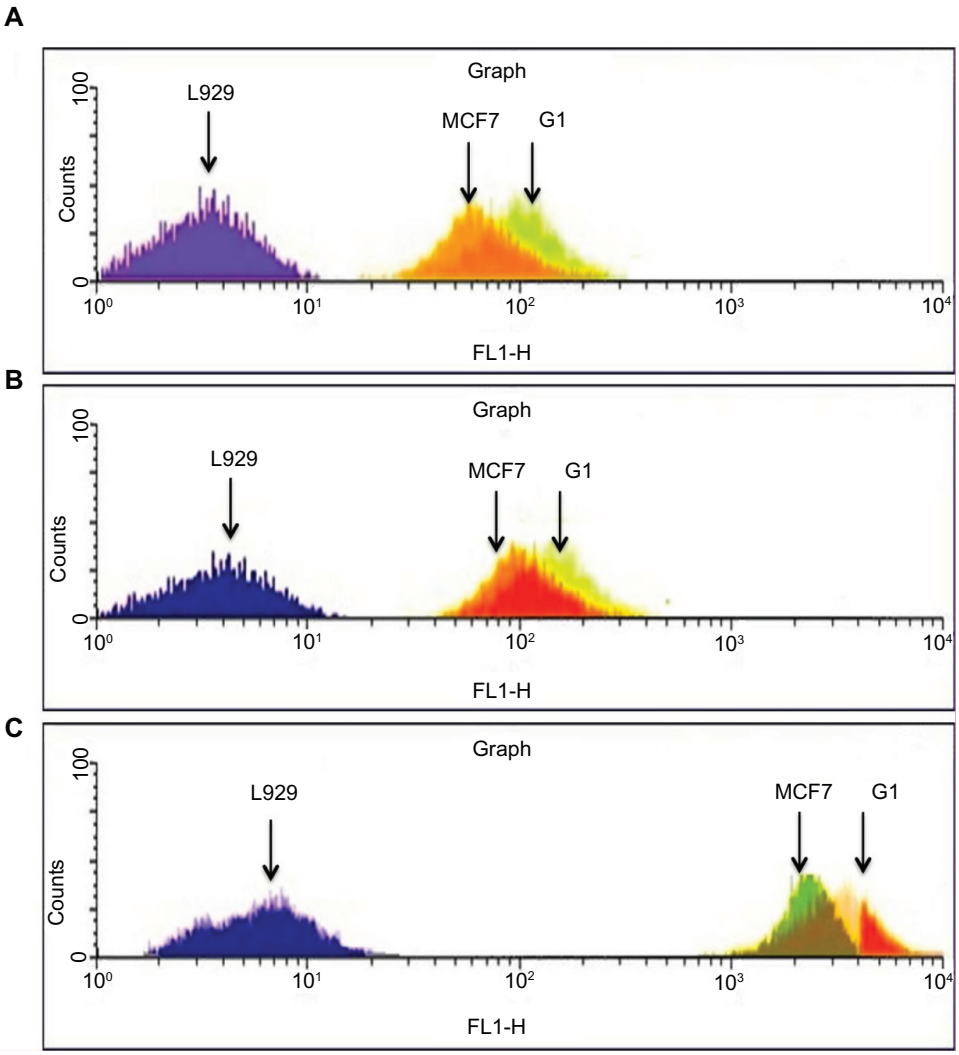

Figure 8 Flow cytometry results.
Notes: Uptake of (**A**) F–Dd–PLGA–MNPs, (**B**) Tf–Dd–PLGA–MNPs, and (**C**) Dt–Dd–PLGA–MNPs in L929, MCF7, and G1 cells.
Abbreviations: F-Dd-PLGA-MNPs, folate targeted double drug loaded magnetic nanoparticle-encapsulated poly(D, L-lactic-co-glycolic acid) nanoparticles; Tf-Dd-PLGA-MNPs, transferrin targeted double drug loaded magnetic nanoparticle-encapsulated poly(D, L-lactic-co-glycolic acid) nanoparticles; Dt-Dd-PLGA-MNPs, double targeted double drug loaded magnetic nanoparticle-encapsulated poly(D, L-lactic-co-glycolic acid) nanoparticles.

with dual-targeted NPs was slightly more than that of the L929 cells with single-targeted NPs. The presence of F and Tf receptors that are normally present in L929 cells might have attributed to the slight increase in the uptake of NPs. However, the flow cytometry and confocal results suggested that the Dt–Dd–PLGA–MNPs were highly specific to the F and Tf receptors that were overexpressed in the cancer cells.

Therapeutic efficiency of the nanoformulation

To investigate the enhanced therapeutic efficiency brought about by the increased cellular uptake of NPs owing to the dual-targeting moieties that were attached to the drug-loaded NPs, time-dependent in vitro alamarBlue cytotoxicity assays were performed. For this analysis, we studied the cytotoxicity assays of the dual-targeted single-drug nanoformulation (Dt-Cur-PLGA-MNPs and Dt–5FU–PLGA–MNPs), the nontargeted dual-drug-loaded nanoformulation (curcumin–5FU–PLGA–MNPs), and Dt–Dd–PLGA–MNPs in the cancer cell lines (MCF7 and G1) and control cell line (L929). When the MCF7 and G1 cell lines were subjected to both dual-targeted single-drug-loaded nanoformulation and the nontargeted dual-drug-loaded nanoformulation, they rendered more or less similar levels of toxicity to the cells at all concentrations. This could be attributed to the enhanced internalization of these nanomaterials by the cancer cells, which was demonstrated from the confocal studies. In the case of Dt–Dd–PLGA–MNPs, both cancer cell lines showed a higher therapeutic efficiency than the dual-targeted single-drug-loaded nanoformulation in all concentrations tested, signifying the therapeutic potential of curcumin and 5FU used together (Figure 9B and C). Meanwhile, when the NPs were treated with the control cell line (L929), we observed minimal cell death when compared to the cancer cells (Figure 9A). The minimal toxicity of the NPs in L929 may be due to their reduced internalization of NPs into the cells. However, the dual-drug-loaded NPs (nontargeted) rendered slight toxicity to the control cells at higher concentrations, which could be attributed to the release of the drugs from the PLGA NPs within 96 hours. The cell death observed in L929 cells when treated with the nontargeted nanoformulation can be attributed to the release of the drug that enters the cell via passive diffusion. However, the cell viability was more when the L929 cells were incubated with the dual-targeted, dual-drug-loaded nanoformulation. The observed results signify and reconfirm, beyond any doubt, the targeting and therapeutic efficiency of double-targeted double-drug-loaded NPs to the cancer cells.

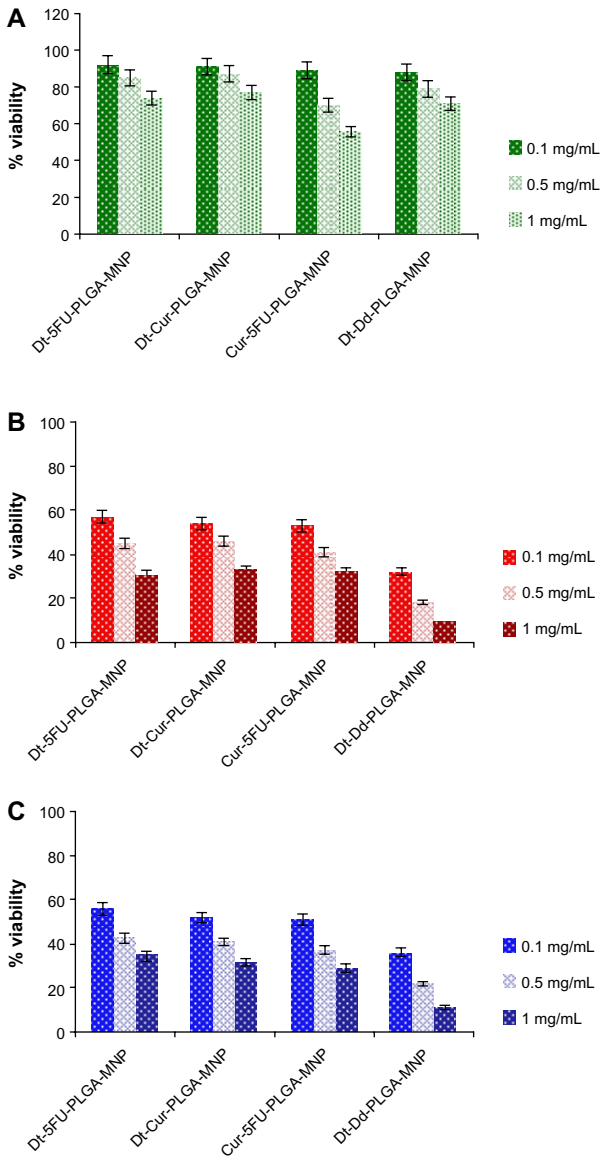

Figure 9 Therapeutic potential of nanodrug formulations (Dt–Cur–PLGA–MNPs, Dt–5FU–PLGA–MNPs, Cur–5FU–PLGA–MNPs, and Dt–Dd-PLGA–MNPs).
Note: (**A**) Control L929 cells, (**B**) human breast adenocarinoma cells (MCF7), and (**C**) human glial cells (G1) represented as bar diagrams.
Abbreviations: Dt–Cur–PLGA–MNPs, double-targeted curcumin magnetic nanoparticle-encapsulated poly(D,L-lactic-co-glycolic acid) nanoparticles; Dt–5FU–PLGA–MNPs, double-targeted 5-Fluorouracil magnetic nanoparticle-encapsulated poly(D,L-lactic-co-glycolic acid) nanoparticles; Cur–5FU–PLGA–MNPs, curcumin–5-Fluorouracil magnetic nanoparticle-encapsulated poly(D,L-lactic-co-glycolic acid) nanoparticles; Dt–Dd-PLGA–MNPs, double targeted double drug loaded magnetic nanoparticle-encapsulated poly(D, L-lactic-co-glycolic acid) nanoparticles.

Mode of cellular damage induced by the nanoformulation

The cytotoxicity instigated by the nanodrug formulations can either lead to an apoptotic or necrotic means of cell death. Owing to the inherent toxicity rendered by the potential drugs (curcumin and 5FU), we considered that the cells might have suffered apoptosis by the interruption of vital cellular organ-

elles that are obligatory for the normal function of the cells, such as depolarization of the mitochondria or disruption of the cytoskeleton (collapse of the tubulin and actin components of the cells that had undergone cell apoptosis).

The decrease in the MMP in the cell is considered as one of the principal features to demonstrate the induction of the basic apoptotic pathway. So, to know the effect of Dt–Dd–PLGA–MNPs on the cells that confer the apoptotic pathway, a mitochondrial membrane depolarization study was done in both MCF7 and G1 cell lines by using cationic JC-1.[56] The study of the loss of MMP by Dt–Dd–PLGA–MNPs in MCF7 and G1 cells was analyzed by confocal imaging (Figure 10). It was established that during apoptosis, the mitochondrial permeability transition pores that are present inside the mitochondria, specifically in the inner mitochondrial membrane, open up.[57–60] This situation that occurs inside the inner membrane of the mitochondria allows for the redistribution of molecules across the inner mitochondrial membrane, which leads to the loss of MMP. The results showed that drug-loaded NPs demonstrated an inhibition of the formation of JC aggregates, demonstrating a loss of $\Delta\Psi m$ that was observed as green fluorescence in the confocal results. Thus, the F and Tf conjugated dual-drug-loaded PLGA–MNPs presented apoptotic cell populations owing to the accumulation and sustained release of the drug from the nanoformulation, thus showing the therapeutic efficacy in malignant cancer cells. A combination of curcumin and 5FU resulted in membrane depolarization due to combined action of both of the drugs simultaneously in cancer cells.

Damage to the cytoskeleton as a result of apoptosis, which was induced by Dt–Dd–PLGA–MNPs, was also investigated by confocal microscopy in MCF7 and G1 cells. We observed that the rigidity and the structure of actin and tubulin microfilaments were completely lost when the cells were treated with the nanoformulation (Figure 11). The majority of the cells exhibited a shrunken morphology with crumbled actin filaments. The disruption of the actin and tubulin cytoskeleton is another major indicator of the induction of apoptosis, which leads to the death of cells.[61,62] The cells were totally shriveled and exhibited horseshoe-shaped nuclei, which are distinctive of apoptotic cell death.

We could also observe several membrane blebs with small vesicles, often known as apoptotic bodies, which can be clearly visualized from phase contrast images (Figure 12). A set of confocal images (Figure 13A and B) that clearly showed the different stages of apoptosis in MCF7 and G1 are provided in bright field images from the confocal microscope. Distinctive change in cellular morphology leading to shrunken structure, membrane blebbings, nuclear condensation, and the appearance of blisters can be clearly seen from the confocal images. These structures are often

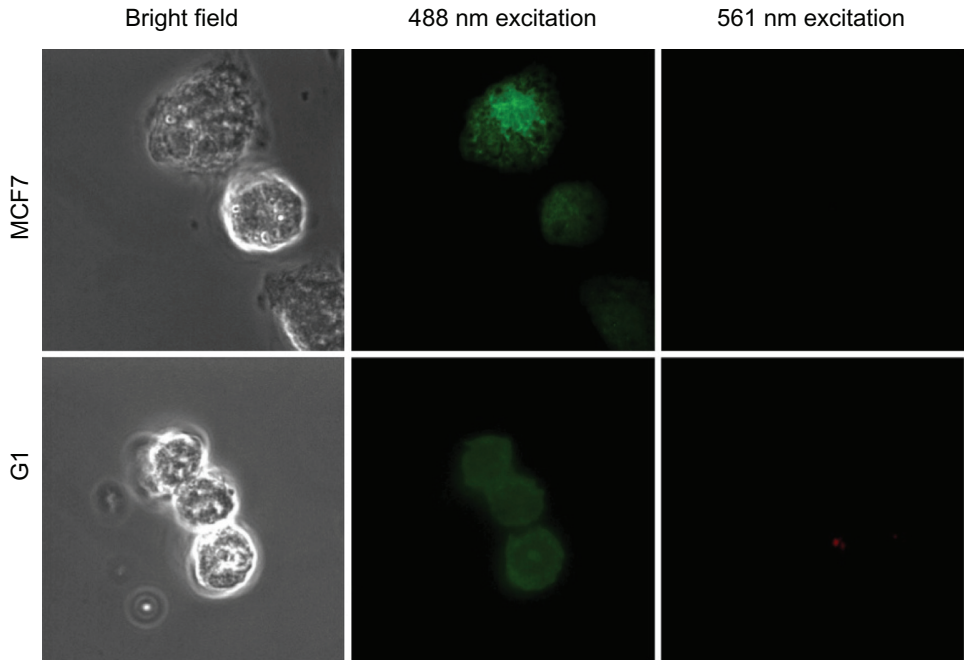

Figure 10 Confocal images of MCF7 and G1 cells displaying the loss of MMP induced by Dt–Dd–PLGA–MNPs.
Abbreviations: MMP, mitochondrial membrane potential; Dt–Dd–PLGA–MNPs, double targeted double drug loaded magnetic nanoparticle-encapsulated poly (D, L-lactic-co-glycolic acid) nanoparticles.

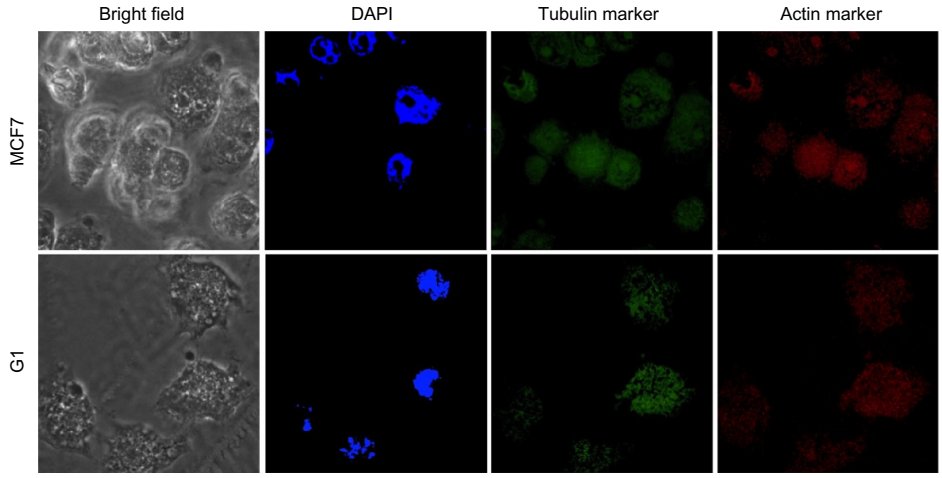

Figure 11 Actin and microtubulin staining of Dt–Dd–PLGA–MNP treated MCF7 and G1 cells.
Notes: The normal cellular morphology was lost with highly destabilized actin and microtubulin. Nuclei stained with DAPI displayed a horseshoe structure, indicating the symptoms of apoptosis.
Abbreviations: DAPI, 4′6,-diamidino-2-phenylindole dihydrochloride; Dt–Dd–PLGA–MNPs, double targeted double drug loaded magnetic nanoparticle-encapsulated poly(D, L-lactic-co-glycolic acid) nanoparticles.

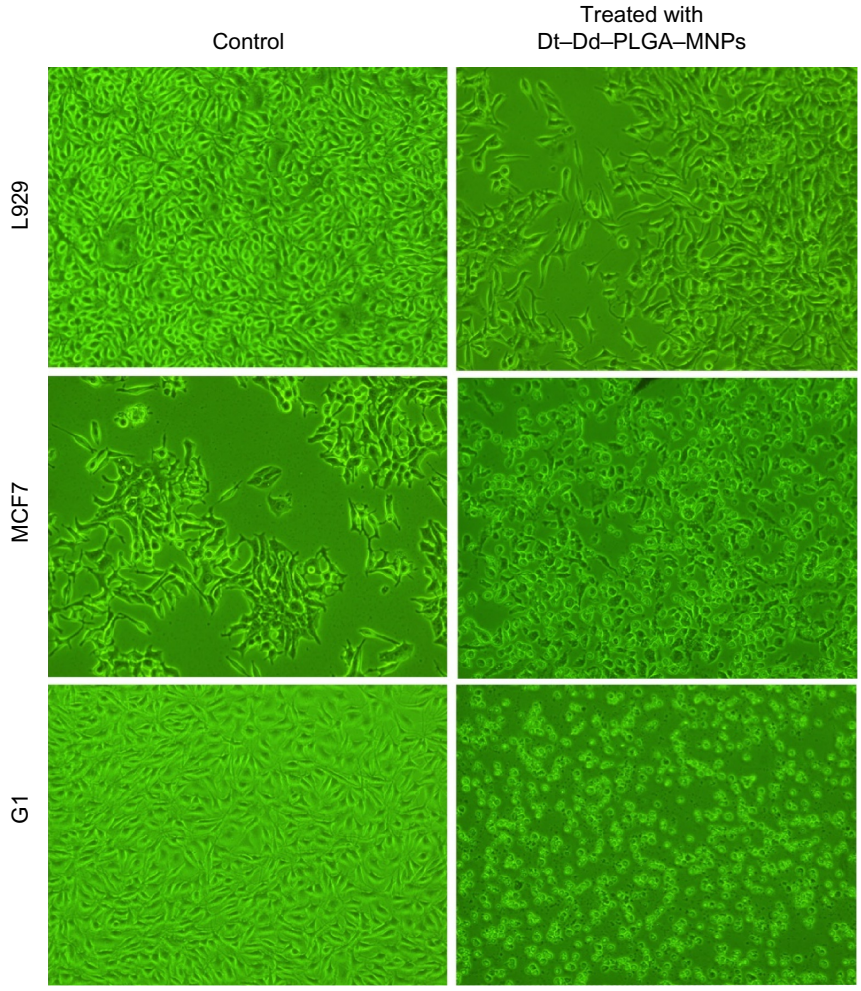

Figure 12 Phase contrast images of Dt–Dd–PLGA–MNP-treated cells.
Notes: The control cells (L929) show healthy growing cells, whereas MCF7 and G1 cells display apoptotic behavior. The cancer cells were dead by 96 hours of nanoformulation exposure, whereas the control (L929) cells treated with the nanoformulation were highly viable with negligible cytotoxic effects.
Abbreviation: Dt–Dd–PLGA–MNP, double targeted double drug loaded magnetic nanoparticle-encapsulated poly(D, L-lactic-co-glycolic acid) nanoparticles.

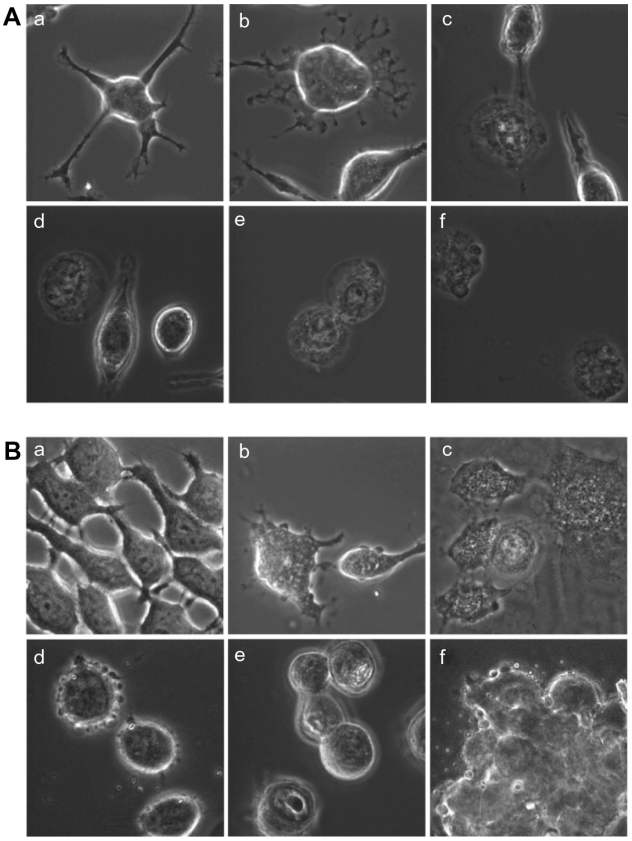

Figure 13 Confocal (bright field) images of different stages of apoptosis induced by Dt–Dd–PLGA–MNPs on G1 cells and MCF7 cells.
Notes: (**A**) G1 cells and (**B**) MCF7 cells. As observed from the confocal images, upon treatment with the nanoformulation, the normal morphology of the cells was changed with the appearance of several membrane blebs, finally leading to cell death.
Abbreviation: Dt–Dd–PLGA–MNPs, double-targeted magnetic nanoparticle-encapsulated poly(D,L-lactic-co-glycolic acid) nanoparticles.

characterized during the end stages of apoptosis. These results demonstrate the superiority of the dual-targeted and dual-drug-loaded NPs against cancer, thus increasing the prospects that these nanoformulations can be used for in vivo applications.

In addition, the synergistic effect of the double-drug nanoformulations further confirmed the results of the apoptosis study by Annexin V-PI. The synergistic effect of dual-drug-loaded PLGA–MNPs might be due to the activation of apoptosis, which is related to the loss of the MMP, damage to the cytoskeleton, along with several other events that finally led to cell death.

Apoptosis induced by the nanoformulation

We have further analyzed apoptosis to confirm the results from the MMP loss and cytoskeletal damage induced by the Dt–Dd–PLGA–MNPs. For this, we studied the effect of Dt–Dd–PLGA–MNPs on MCF7, G1, and L929 cells after 96 hours of treatment using an Annexin V-PI protocol by flow cytometry. The Annexin V-PI assay is based on the fact that just after the induction of apoptosis, phosphatidylserine is translocated from the inner plasma membrane to the outer leaflet. Since Annexin V has a strong affinity for phosphatidylserine, it binds to and detects the apoptotic cell population (the confocal observations are shown in Figure 14A). The flow cytometry result (Figure 14B) revealed the existence of a substantial portion of early apoptotic and late apoptotic cell populations following treatment with Dt–Dd–PLGA–MNPs in MCF7 and G1 cells. We have observed early apoptosis in 25.82% of MCF7 cells and 17.78% of G1 cells, and late apoptosis in 69.37% of MCF7 cells and 77.76% of G1 cells. However, the apoptotic cell population in L929 was 1.91%, indicating the effectiveness of Dt–Dd–PLGA–MNPs, thus sparing the normal cells.

Magnetic hyperthermia studies on cancer cells

MNPs have substantial potential for their application in hyperthermia treatment for cancer. We have performed drug release from PLGA MNPs under MHT, and the results are provided in Figure 15A. We have observed an increase in the percentage of drug release (both for 5FU and curcumin) under a magnetic field when compared to control cells (the sample that was not exposed to the magnetic field). To examine whether our nanoformulation (MNP, PLGA–MNP, Dd–PLGA–MNPs, and Dt–Dd–PLGA–MNPs) are ideal candidates for MHT, experiments were carried out in cancer cells (MCF7 and G1) and control cells (L929). The treatment was performed for 60 minutes and 120 minutes with Dd–PLGA–MNPs and Dt–Dd–PLGA–MNPs in the cells. The exposure of the cells to the magnetic field in the absence of NPs did not show any substantial cytotoxic effect on cell viability, clearly indicating that magnetic field exposure does not cause any damage to the cells (data not shown). The potential of MHT with MNP and PLGA–MNP was confirmed with the reduction of cell viability. We found that the cellular viability was greater in the L929 cells compared to the cancer cells. This may be attributed to the healthy nature of the normal cells when compared to the cancer cells. The nontargeted double-drug-loaded nanoformulation was highly cytotoxic to both the control cells and the cancer cells, owing to the nonspecificity of the nanoformulation (Figure 15B). However, when the cells were treated with the targeted nanoformulation (Dt–Dd–PLGA–MNPs) in the presence of the AC magnetic field for a period of 60 minutes

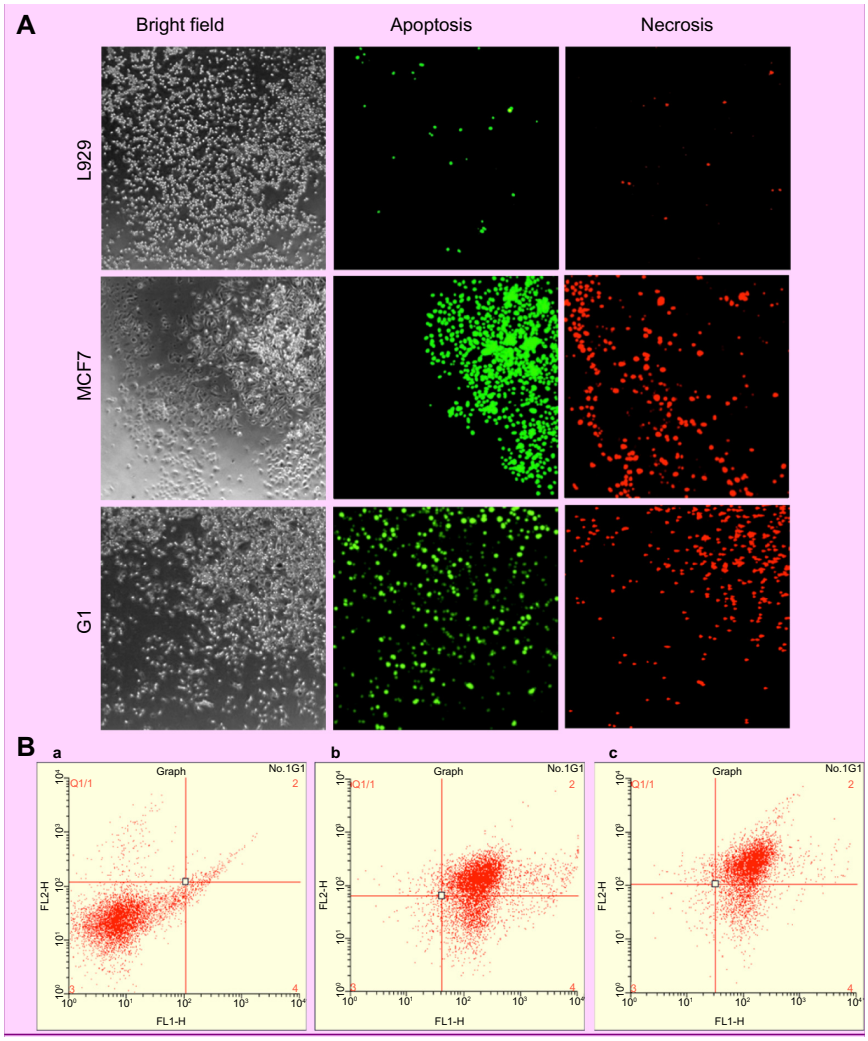

Figure 14 Confocal images and flow cytometry results of L929, MCF7, and G1 cells after treatment with Dt–Dd–PLGA–MNPs.
Notes: (**A**) Confocal images of Annexin V-PI staining on L929, MCF7, and G1 cells after treatment with Dt–Dd–PLGA–MNPs. (**B**) Flow cytometry results of L929, MCF7, and G1 cells after treatment with Dt–Dd–PLGA–MNPs. Both results display the presence of early apoptotic and late apoptotic cells, indicating the therapeutic potential of Dt–Dd–PLGA–MNPs.
Abbreviation: Dt–Dd–PLGA–MNPs, double targeted double drug loaded magnetic nanoparticle-encapsulated poly(D, L-lactic-co-glycolic acid) nanoparticles.

and 120 minutes, the viability of the cancer cells reduced drastically (Figure 15B).

To confirm the cell viability after hyperthermia treatment, we trypsinized the cells. To the cell pellet, Trypan blue was added and the viable cells were counted via Countess (Life Technologies Carlsbad, CA, USA). We observed that the cell cytotoxicity of Dt–Dd–PLGA–MNPs with MHT for 60 minutes was 41% and 38% for the MCF7 and G1 cells, respectively. However, the cell viability decreased considerably when the cells were given MHT for 120 minutes. We observed a cell viability of 28% and 26% for the MCF7 and G1 cells, respectively. MHT might have triggered the release of the drug from the PLGA, resulting in increased cell death when treated for 120 minutes. Also, since the NPs were tagged with two potent targeting moieties (F and Tf), the chance of uptake of NP by the cancer cells could be much greater because the cancer cells possess numerous F and Tf receptors. We checked the effect of incubation after MHT treatment in MCF7 and G1 cells, and we found a considerable decrease in cellular viability. Cells that were subjected to MHT for 120 minutes were further incubated. The viability accessed just after 120 minutes of MHT was considered as 0h, and it was 28% and 26% for MCF7 and G1 cells, respectively. The cellular viability was further checked at 12 hours and 24 hours of incubation. After 12 hours of incubation, the cell viability decreased to 16% and 11% for the MCF7 and G1 cells, respectively; this was almost comparable to the results obtained from the cytotoxicity assay by alamarBlue with the NPs (Figure 15C). We further extended the incubation period, and after 24 hours, the cell viability

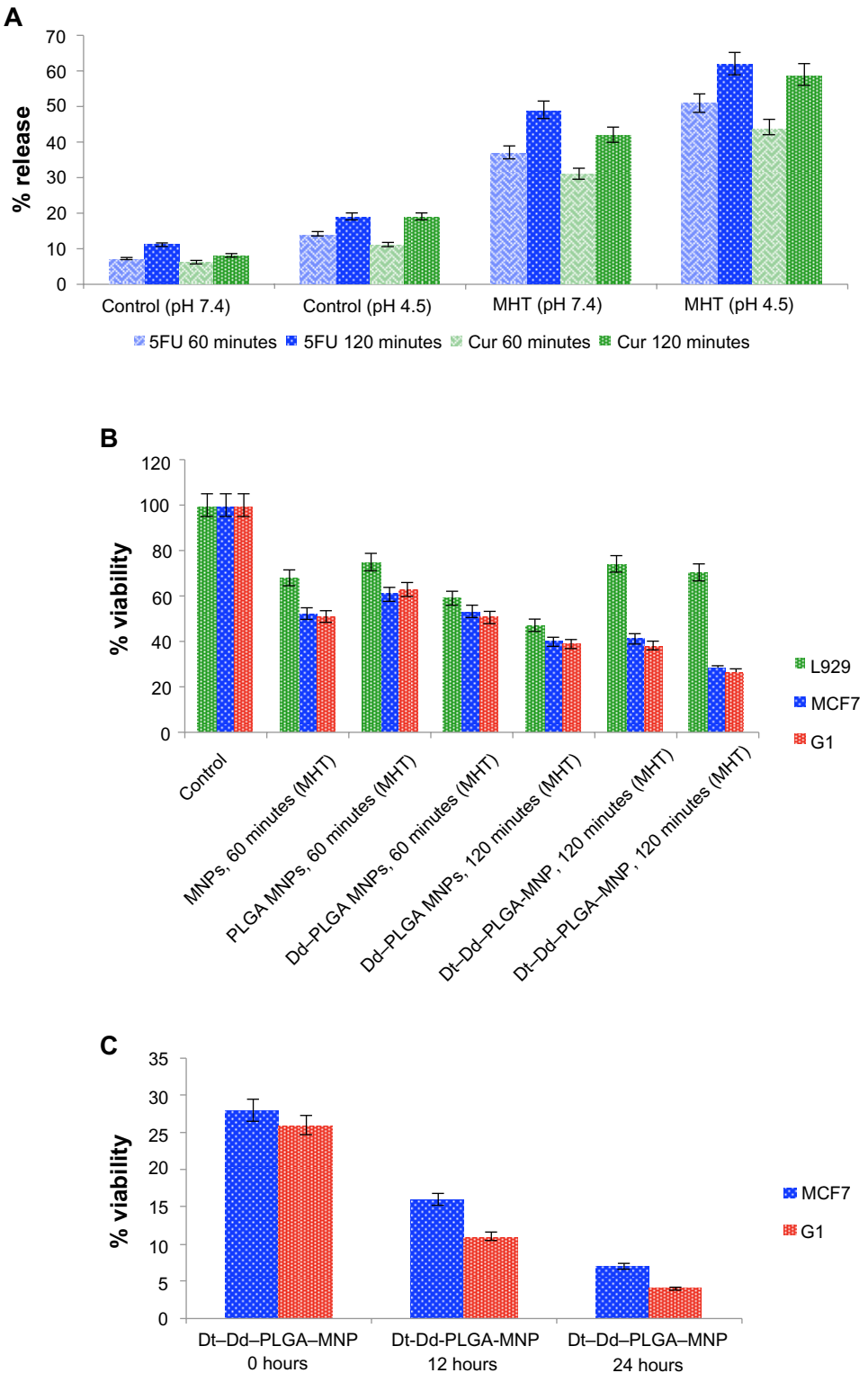

Figure 15 Drug release studies, MHT study, and effect of MHT on the viability of MCF7 and G1 cells.

Notes: (**A**) Drug release studies under a magnetic field at pH levels of 7.4 and 4.5. (**B**) MHT study of different nanoformulations in control cells (L929) and cancer cells (MCF7 and G1 cells) under an alternating magnetic field for HT treatment; the viability was assessed by Trypan blue staining. (**C**) Effect of MHT on the viability of MCF7 and G1 cells at different incubation periods.

Abbreviations: 5FU, 5-Fluorouracil; Cur, curcumin; MNPs, magnetic nanoparticles; MHT, magnetic hyperthermia treatment; PLGA, poly(D,L-lactic-co-glycolic acid); Dd-PLGA-MNPs, double drug loaded magnetic nanoparticle-encapsulated poly(D, L-lactic-co-glycolic acid) nanoparticles; Dt-Dd-PLGA-MNPs, double targeted double drug loaded magnetic nanoparticle-encapsulated poly(D, L-lactic-co-glycolic acid) nanoparticles.

was 7% and 4% in the MCF7 and G1 cells, respectively. We consider that HT treatment resulted in immediate cell death after exposure to the magnetic field, but a small percentage of the cells survived. The surviving injured cells could not recuperate from the impairment induced by HT, owing to the combined action of the curcumin and 5FU present in the PLGA NP. During HT, the drugs might have diffused and resulted in cell death upon incubation. We propose that these could be the probable reasons for the cell death observed during incubation. Also, these results strongly suggest that the MHT application, along with the combination of targeted drugs, can work as an effectual nanotool to target heat to cancer-affected parts, thus considerably overcoming the present challenges associated with traditional HT treatments to maximally kill cancer cells.

Cytoskeletal damage induced upon MHT

To understand the mechanism of cell death induced by MHT with targeted nanoformulations, confocal microscopy analysis of the cells was performed. In the presence of an alternating magnetic field, the morphology of the cancer cells changed considerably.[63–65] We could observe several membrane blebs of various sizes after field exposure of 120 minutes. The blebbings were characterized by the presence of tubulin accumulation, as detected by the enhanced fluorescence of the tubulin staining, which was considered a strong indication of the induction of apoptosis. Parallel to the disruption of the microtubules, the actin filaments were also significantly affected by the MHT treatment (Figure 16). Most of the cells exhibited disintegrated actin filaments and shrunken morphology. The disruption of the actin and tubulin cytoskeleton is considered as one of the hallmarks of the induction of apoptosis leading to the death of cells. The steady decline in the cellular viability of the treated cells based on Trypan blue staining and LIVE/DEAD staining strongly supports the proposal that cytoskeletons of the nanoformulation-treated cells were disturbed, and that the death signal was initiated upon MHT.

LIVE/DEAD assay after MHT

We used a LIVE/DEAD cytotoxicity kit for the qualitative determination of live and dead cells after MHT treatment with Dt–Dd–PLGA–MNPs in MCF7 and G1 cells. MHT with Dt–Dd–PLGA–MNPs results in the death of cancer cells by inducing both necrosis and apoptosis.[66–69] We observed significant cell death as a result of MHT treatment, and the cell death was augmented significantly when curcumin and 5FU were loaded into PLGA NPs. The LIVE/DEAD assay takes advantage of the fact that calcein (the assay's reagent) was retained within the live cells, producing an intense uniform green fluorescence in the live cells. On the other hand EthD-1 (another assay reagent) penetrated into the damaged cell membranes and exhibited bright red fluorescence upon binding to the nucleic acids. As a result of MHT, the cancer cells experienced sudden shock within a short period of time, leading to cellular damage. We also consider that, owing to the heat generated by the MNPs and the enhanced release of the drug from the NPs during MHT, huge stress was generated inside the cell, which broke down almost all vital cellular

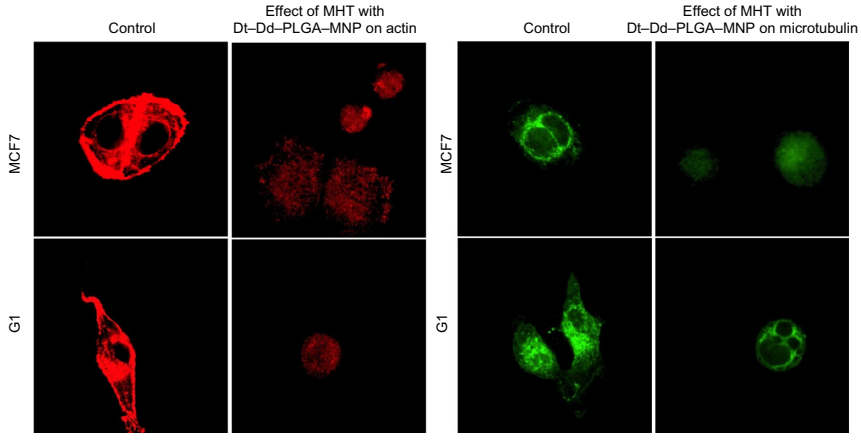

Figure 16 Confocal images of cytoskeletal staining with actin and microtubulin markers in control cells (before MHT) and cells after MHT with Dt–Dd–PLGA–MNP.
Notes: The control cells devoid of the nanoformulation, before MHT treatment, displayed the normal tubulin and actin architecture, whereas the cells subjected to MHT showed shrunken cellular morphology, highly destabilized actin and microtubulin, leading to apoptotic symptoms.
Abbreviations: MHT, magnetic hyperthermia treatment; Dt–Dd–PLGA–MNPs, double targeted double drug loaded magnetic nanoparticle-encapsulated poly(D, L-lactic-co-glycolic acid) nanoparticles.

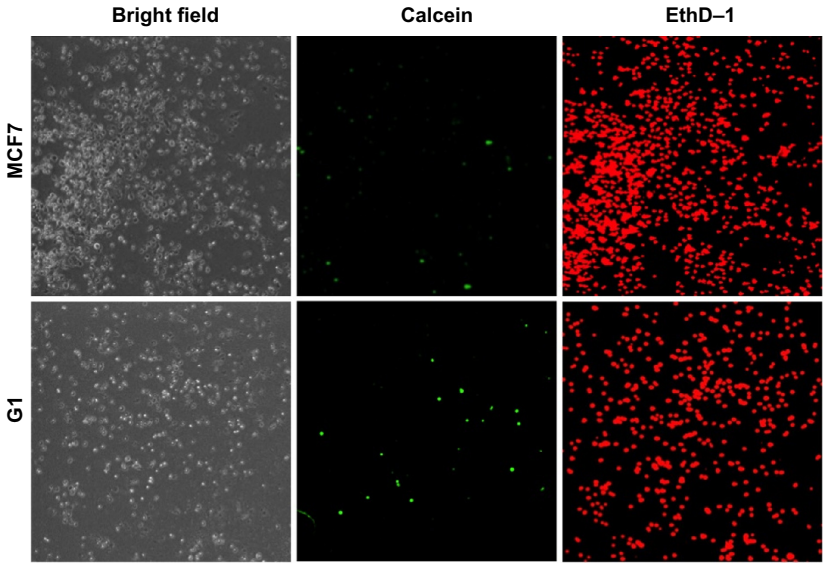

Figure 17 LIVE/DEAD staining after MHT Dt–Dd–PLGA–MNPs on MCF7 and G1 cells, indicating the existence of a higher amount of dead cells.
Abbreviations: MHT, magnetic hyperthermia treatment; Dt–Dd–PLGA–MNPs, double targeted double drug loaded magnetic nanoparticle-encapsulated poly(D, L-lactic-co-glycolic acid) nanoparticles.

activities. The extensive necrosis in Dt–Dd–PLGA–MNP-internalized cancer cells was clearly demonstrated from the EthD-positive staining of the cell populations (Figure 17), confirming the efficacy of these NPs in killing cancer cells. These events might have triggered cell damage, resulting in cancer cell death, as observed in the confocal images. These results affirmed the ability of our nanoconjugate, Dt–Dd–PLGA–MNPs, upon MHT, which leads to the destruction of cancer cells, strengthening the claim that they can be used as potential hyperthermia agents.

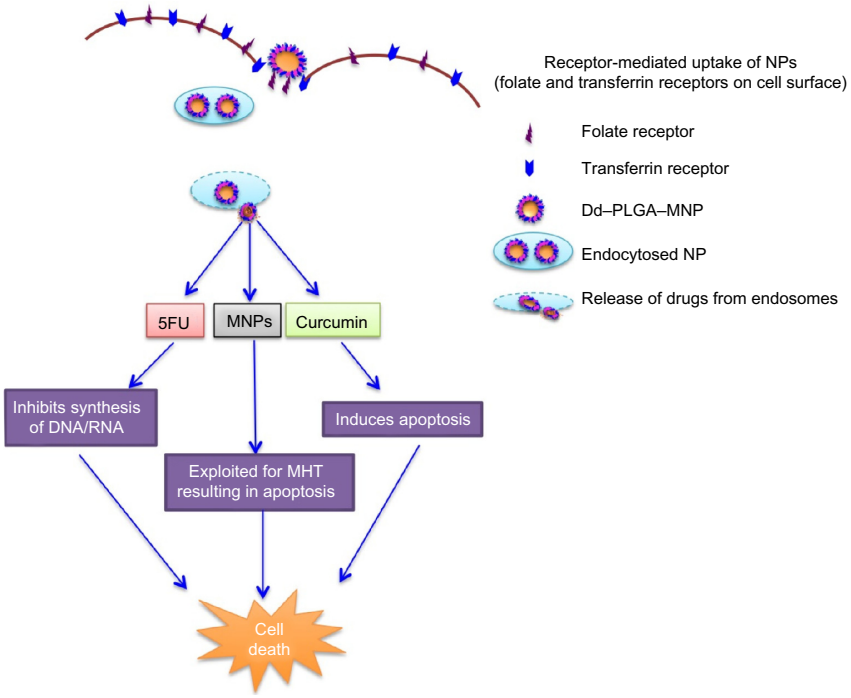

Figure 18 Schematic representation illustrating the possible mechanisms induced by Dt–Dd–PLGA–MNPs on cancer cells upon incubation and after performing MHT.
Abbreviations: NP, nanoparticle; Dd–PLGA–MNP, magnetic nanoparticle-encapsulated poly(D,L-lactic-co-glycolic acid) nanoparticles; 5FU, 5-Fluorouracil; MNPs, magnetic nanoparticles; DNA, deoxyribonucleic acid; RNA, ribonucleic acid; MHT, magnetic hyperthermia treatment; Dt–Dd–PLGA–MNPs, double targeted double drug loaded magnetic nanoparticle-encapsulated poly(D, L-lactic-co-glycolic acid) nanoparticles.

A schematic representation that explains the possible cytotoxic effects rendered by Dt–Dd–PLGA–MNP upon internalization via F and Tf receptors on the cell surface, as well as the release of the drug from the acidic environment of lysosomes is shown in Figure 18. It should be noted that 5FU in the nanoconjugate possibly inhibits cell division by hindering the pathway in nucleic acid synthesis, while curcumin destabilizes the MMP that induces the initiation of apoptosis, thus triggering several pathways involved in apoptosis. Also the NPs collapse the cytoskeletal architecture, yield nuclear condensation, and finally result in cell death. The MNPs encapsulated in the nanoconjugate were exploited for MHT, which also causes cellular damage, triggering the events in apoptosis and finally cell death within a short period of time.

Conclusion

The ultimate goal in cancer therapy is to formulate multifunctional NPs that are tailored to specifically target the cancer cells while sparing the normal healthy neighboring cells. With this aim, we formulated dual-targeted double drug-loaded PLGA–MNPs in this study, which were characterized and evaluated for their efficacy and appropriateness as targeted drug delivery systems. The formulated nanodrug carrier system appeared to deliver drug combinations in a sustained release manner, demonstrating dose-dependent and pH-responsive cytotoxicity in MCF7 and G1 cells. Also, for targeted delivery of a therapeutic payload, we functionalized the nanocarriers with dual-targeting ligands. Our results clearly indicate that curcumin along with 5FU in PLGA NPs resulted in enhanced uptake, cellular accumulation, and greater cytotoxicity in cancer cells. Further, the potential of MHT was studied, in which the synergistic effect of the MNPs and the combination of the drugs was found to be highly effective in destroying cancer cells within a very short period of time, thus triggering enhanced apoptosis. We believe that these fascinating dual-targeted, dual-drug-loaded magnetic nanoformulations served as a potential nanoplatform for highly proficient diagnostic and therapeutic (theragnostic) applications.

Acknowledgments

S Balasubramanian thanks the Rotary Yoneyama Foundation, Japan for providing a fellowship for conducting his doctoral course. Also, part of this study was supported by a grant for the Programme of the Strategic Research Foundation at Private Universities S1101017, organized by the MEXT, Japan since April 2012.

Disclosure

The authors report no conflicts of interest in this work.

References

1. Baselt DR, Lee GU, Hansen KM, Chrisey LA, Colton RJ. A high-sensitivity micromachined biosensor. *Proc IEEE Inst Electr Electron Eng*. 1997;85(4):672–680.
2. Safarík I, Safaríková M. Use of magnetic techniques for the isolation of cells. *J Chromatogr B Biomed Sci Appl*. 1999;722(1–2):33–53.
3. Halbreich A, Roger J, Pons JN, et al. Biomedical applications of maghemite ferrofluid. *Biochimie*. 1999;80(5–6):379–390.
4. Fortin JP, Wilhelm C, Servais J, Ménager C, Bacri JC, Gazeau F. Size-sorted anionic iron oxide nanomagnets as colloidal mediators for magnetic hyperthermia. *J Am Chem Soc*. 2007;129(9):2628–2635.
5. Hergt R, Hiergeist R, Hilger I, et al. Maghemite nanoparticles with very high AC-losses for application in RF-magnetic hyperthermia. *J Magn Magn Mater*. 2004;270(3):345–357.
6. Chemla YR, Grossman HL, Poon Y, et al. Ultrasensitive magnetic biosensor for homogeneous immunoassay. *Proc Natl Acad Sci U S A*. 2000;97(26):14268–14272.
7. Briley-Saebo K, Bjørnerud A, Grant D, Ahlstrom H, Berg T, Kindberg GM. Hepatic cellular distribution and degradation of iron oxide nanoparticles following single intravenous injection in rats: implications for magnetic resonance imaging. *Cell Tissue Res*. 2004;316(3):315–323.
8. Stark DD, Weissleder R, Elizondo G, et al. Superparamagnetic iron oxide: clinical application as a contrast agent for MR imaging of the liver. *Radiology*. 1988;168(2):297–301.
9. Häfeli UO. Magnetically modulated therapeutic systems. *Int J Pharm*. 2004;277(1–2):19–24.
10. Mahmoudi M, Simchi A, Imani M, et al. A new approach for the in vitro identification of the cytotoxicity of superparamagnetic iron oxide nanoparticles. *Colloids Surf B Biointerfaces*. 2010;75(1):300–309.
11. Ito A, Takizawa Y, Honda H, et al. Tissue engineering using magnetite nanoparticles and magnetic force: heterotypic layers of cocultured hepatocytes and endothelial cells. *Tissue Eng*. 2004;10(5–6):833–840.
12. Alexiou C, Schmidt A, Klein R, Hulin P, Bergemann C, Arnold W. Magnetic drug targeting: biodistribution and dependency on magnetic field strength. *J Magn Magn Mater*. 2002;252:363–366.
13. Pan Y, Du X, Zhao F, Xu B. Magnetic nanoparticles for the manipulation of proteins and cells. *Chem Soc Rev*. 2012;41(7):2912–2942.
14. Xu C, Sun S. Superparamagnetic nanoparticles as targeted probes for diagnostic and therapeutic applications. *Dalton Trans*. 2009;(29):5583–5591.
15. Perez CA, Emami B, Myerson RJ. *Hyperthermia: In Principle and Practice of Radiation Oncology*. Philadelphia, PA: Lippincott; 1992.
16. Maier-Hauff K, Rothe R, Scholz R, et al. Intracranial thermotherapy using magnetic nanoparticles combined with external beam radiotherapy: results of a feasibility study on patients with glioblastoma multiforme. *J Neurooncol*. 2007;81(1):53–60.
17. Berry CC, Curtis ASG. Functionalisation of magnetic nanoparticles for applications in biomedicine. *J Phys D Appl Phys*. 2003;36: R198–R206.
18. Gordon RT, Hines JR, Gordon D. Intracellular hyperthermia. A biophysical approach to cancer treatment via intracellular temperature and biophysical alterations. *Med Hypotheses*. 1979;5(1):83–102.
19. Hilger I, Andrä W, Hergt R, Hiergeist R, Schubert H, Kaiser WA. Electromagnetic heating of breast tumors in interventional radiology: in vitro and in vivo studies in human cadavers and mice. *Radiology*. 2001;218(2):570–575.
20. Dormer K, Seeney C, Lewelling K, Lian G, Gibson D, Johnson M. Epithelial internalization of superparamagnetic nanoparticles and response to external magnetic field. *Biomaterials*. 2005;26(14):2061–2072.
21. Murray TG, Steeves RA, Gentry L, et al. Ferromagnetic hyperthermia: functional and histopathologic effects on normal rabbit ocular tissue. *Int J Hyperthermia*. 1997;13(4):423–436.

22. Jordan A, Scholz R, Wust P, et al. Effects of magnetic fluid hyperthermia (MFH) on C3H mammary carcinoma in vivo. *Int J Hyperthermia*. 1997;13(6):587–605.
23. O'Brien KT, Mekkaoui AM. Numerical simulation of the thermal fields occurring in the treatment of malignant tumors by local hyperthermia. *J Biomech Eng*. 1993;115(3):247–253.
24. Chen JS, Poirier DR, Damento MA, Demer LJ, Biancaniello F, Cetas TC. Development of Ni-4 wt% Si thermoseeds for hyperthermia cancer treatment. *J Biomed Mater Res*. 1988;22(4):303–319.
25. Brezovich IA. Low frequency hypothermia: capacitive and ferromagnetic thermoseed methods. In: Palival PR, Hetzel FW, editors. *Medical Physics Monograph*. New York, NY: American Institute of Physics; 1988:82–111.
26. Cullity BD. *Introduction to Magnetic Materials*. Reading, MA: Addison-Wesley; 1972.
27. Esmaeili F, Ghahremani MH, Esmaeili B, Khoshayand MR, Atyabi F, Dinarvand R. PLGA nanoparticles of different surface properties: preparation and evaluation of their body distribution. *Int J Pharm*. 2008;349(1–2):249–255.
28. Shive MS, Anderson JM. Biodegradation and biocompatibility of PLA and PLGA microspheres. *Adv Drug Deliv Rev*. 1997;28(1):5–24.
29. Singh A, Dilnawaz F, Mewar S, Sharma U, Jagannathan NR, Sahoo SK. Composite polymeric magnetic nanoparticles for co-delivery of hydrophobic and hydrophilic anticancer drugs and MRI imaging for cancer therapy. *ACS Appl Mater Interfaces*. 2011;3(3):842–856.
30. Ringman JM, Frautschy SA, Cole GM, Masterman DL, Cummings JL. A potential role of the curry spice curcumin in Alzheimer's disease. *Curr Alzheimer Res*. 2005;2(2):131–136.
31. Ravindran J, Prasad S, Aggarwal BB. Curcumin and cancer cells: how many ways can curry kill tumor cells selectively? *AAPS J*. 2009; 11(3):495–510.
32. Aggarwal BB, Kumar A, Bharti AC. Anticancer potential of curcumin: preclinical and clinical studies. *Anticancer Res*. 2003;23(1A): 363–398.
33. Cartiera MS, Ferreira EC, Caputo C, Egan ME, Caplan MJ, Saltzman WM. Partial correction of cystic fibrosis defects with PLGA nanoparticles encapsulating curcumin. *Mol Pharm*. 2010;7(1):86–93.
34. Goel A, Kunnumakkara AB, Aggarwal BB. Curcumin as "Curecumin": from kitchen to clinic. *Biochem Pharmacol*. 2008;75(4):787–809.
35. Corson TW, Crews CM. Molecular understanding and modern application of traditional medicines: triumphs and trials. *Cell*. 2007;130(5):769–774.
36. Golombick T, Diamond TH, Badmaev V, Manoharan A, Ramakrishna R. The potential role of curcumin in patients with monoclonal gammopathy of undefined significance – its effect on paraproteinemia and the urinary N-telopeptide of type I collagen bone turnover marker. *Clin Cancer Res*. 2009;15(18):5917–5922.
37. Kunnumakkara AB, Anand P, Aggarwal BB. Curcumin inhibits proliferation, invasion, angiogenesis and metastasis of different cancers through interaction with multiple cell signaling proteins. *Cancer Lett*. 2008;269(2):199–225.
38. Tharakan ST, Inamoto T, Sung B, Aggarwal BB, Kamat AM. Curcumin potentiates the antitumor effects of gemcitabine in an orthotopic model of human bladder cancer through suppression of proliferative and angiogenic biomarkers. *Biochem Pharmacol*. 2010; 79(2):218–228.
39. Kuttan R, Sudheeran PC, Josph CD. Turmeric and curcumin as topical agents in cancer therapy. *Tumori*. 1987;73(1):29–31.
40. Cho YW, Lee JR, Song SC. Novel thermosensitive 5-fluorouracil-cyclotriphosphazene conjugates: synthesis, thermosensitivity, degradability, and in vitro antitumor activity. *Bioconjug Chem*. 2005;16(6):1529–1535.
41. Chen AZ, Pu XM, Kang YQ, Liao L, Yao YD, Yin GF. Preparation of 5-fluorouracil-poly(L-lactide) microparticles using solution-enhanced dispersion by supercritical CO2. *Macromol Rapid Commun*. 2006;27(15):1254–1259.
42. Hong H, Yang K, Zhang Y, et al. In vivo targeting and imaging of tumor vasculature with radiolabeled, antibody-conjugated nanographene. *ACS Nano*. 2012;6(3):2361–2370.
43. Sasidharan A, Chandran P, Menon D, Raman S, Nair S, Koyakutty M. Rapid dissolution of ZnO nanocrystals in acidic cancer microenvironment leading to preferential apoptosis. *Nanoscale*. 2011;3(9): 3657–3669.
44. Moghimi SM, Peer D, Langer R. Reshaping the future of nanopharmaceuticals: ad iudicium. *ACS Nano*. 2011;5(11):8454–8458.
45. Xiao Z, Levy-Nissenbaum E, Alexis F, et al. Engineering of targeted nanoparticles for cancer therapy using internalizing aptamers isolated by cell-uptake selection. *ACS Nano*. 2012;6(1):696–704.
46. Perfézou M, Turner A, Merkoçi A. Cancer detection using nanoparticle-based sensors. *Chem Soc Rev*. 2012;41(7):2606–2622.
47. Mulik RS, Mönkkönen J, Juvonen RO, Mahadik KR, Paradkar AR. Transferrin mediated solid lipid nanoparticles containing curcumin: enhanced in vitro anticancer activity by induction of apoptosis. *Int J Pharm*. 2010;398(1–2):190–203.
48. Sahoo SK, Ma W, Labhasetwar V. Efficacy of transferrin-conjugated paclitaxel-loaded nanoparticles in a murine model of prostate cancer. *Int J Cancer*. 2004;112(2):335–340.
49. Mohanty C, Sahoo SK. The in vitro stability and in vivo pharmacokinetics of curcumin prepared as an aqueous nanoparticulate formulation. *Biomaterials*. 2010;31(25):6597–6611.
50. Pan J, Feng SS. Targeting and imaging cancer cells by folate-decorated, quantum dots (QDs)-loaded nanoparticles of biodegradable polymers. *Biomaterials*. 2009;30(6):1176–1183.
51. Mohapatra S, Pal D, Ghosh SK, Pramanik P. Design of superparamagnetic iron oxide nanoparticle for purification of recombinant proteins. *J Nanosci Nanotechnol*. 2007;7(9):3193–3199.
52. Sivakumar B, Aswathy RG, Nagaoka Y, et al. Multifunctional carboxymethyl cellulose-based magnetic nanovector as a theragnostic system for folate receptor targeted chemotherapy, imaging, and hyperthermia against cancer. *Langmuir*. 2013;29(10):3453–3466.
53. Dilnawaz F, Singh A, Sahoo SK. Transferrin-conjugated curcumin-loaded superparamagnetic iron oxide nanoparticles induce augmented cellular uptake and apoptosis in K562 cells. *Acta Biomater*. 2012;8(2):704–719.
54. Kim DH, Lee SH, Im KH, et al. Surface-modified magnetite nanoparticles for hyperthermia: preparation, characterization, and cytotoxic studies. *Curr Appl Phys*. 2006;6(Suppl 1):e242–e246.
55. Gonçalves C, Pereira P, Gama M. Self-assembled hydrogel nanoparticles for drug delivery applications. *Materials (Basel)*. 2010;3(2):1420–1460.
56. Avellino R, Romano S, Parasole R, et al. Rapamycin stimulates apoptosis of childhood acute lymphoblastic leukemia cells. *Blood*. 2005;106(4):1400–1406.
57. Zamzami N, Susin SA, Marchetti P, et al. Mitochondrial control of nuclear apoptosis. *J Exp Med*. 1996;183(4):1533–1544.
58. Cossarizza A, Baccarani-Contri M, Kalashnikova G, Franceschi C. A new method for the cytofluorimetric analysis of mitochondrial membrane potential using the J-aggregate forming lipophilic cation 5,5′,6,6′-tetrachloro-1,1′,3,3′-tetraethylbenzimidazolcarbocyanine iodide (JC-1). *Biochem Biophys Res Commun*. 1993;197(1): 40–45.
59. Bernardi P, Petronilli V. The permeability transition pore as a mitochondrial calcium release channel: a critical appraisal. *J Bioenerg Biomembr*. 1996;28(2):131–138.
60. Zoratti M, Szabó I. Electrophysiology of the inner mitochondrial membrane. *J Bioenerg Biomembr*. 1994;26(5):543–553.
61. Mashima T, Naito M, Noguchi K, Miller DK, Nicholson DW, Tsuruo T. Actin cleavage by CPP-32/apopain during the development of apoptosis. *Oncogene*. 1997;14(9):1007–1012.
62. Luchetti F, Mannello F, Canonico B, et al. Integrin and cytoskeleton behaviour in human neuroblastoma cells during hyperthermia-related apoptosis. *Apoptosis*. 2004;9(5):635–648.

63. Willingham MC. Cytochemical methods for the detection of apoptosis. *J Histochem Cytochem*. 1999;47(9):1101–1110.
64. Borrelli MJ, Wong RS, Dewey WC. A direct correlation between hyperthermia-induced membrane blebbing and survival in synchronous G1 CHO cells. *J Cell Physiol*. 1986;126(2):181–190.
65. Prasad NK, Rathinasamy K, Panda D, Bahadur D. Mechanism of cell death induced by magnetic hyperthermia with nanoparticles of γ-MnxFe2-xO3 synthesized by a single step process. *J Mater Chem*. 2007;17(48):5042–5051.
66. Rodríguez-Luccioni HL, Latorre-Esteves M, Méndez-Vega J, et al. Enhanced reduction in cell viability by hyperthermia induced by magnetic nanoparticles. *Int J Nanomedicine*. 2011;6:373–380.
67. Asín L, Ibarra MR, Tres A, Goya GF. Controlled cell death by magnetic hyperthermia: effects of exposure time, field amplitude, and nanoparticle concentration. *Pharm Res*. 2012;29(5):1319–1327.
68. Hwang SY, Cho SH, Lee BH, Song YJ, Lee EK. Cellular imaging assay for early evaluation of an apoptosis inducer. *Apoptosis*. 2011;16(10):1068–1075.
69. Garcia MP, Cavalheiro JR, Fernandes MH. Acute and long-term effects of hyperthermia in B16-F10 melanoma cells. *PLoS One*. 2012;7(4):e35489.